Differentiation Paths of Peyer's Patch LysoDCs Are Linked to Sampling Site Positioning, Migration, and T Cell Priming

Camille Wagner, Johnny Bonnardel, Clément da Silva, Lionel Spinelli, Cynthia Arroyo Portilla, Julie Tomas, Margaux Lagier, Lionel Chasson, Marion Massé, Marc Dalod, et al.

Article

Cell Reports

Differentiation Paths of Peyer's Patch LysoDCs Are Linked to Sampling Site Positioning, Migration, and T Cell Priming

Graphical Abstract

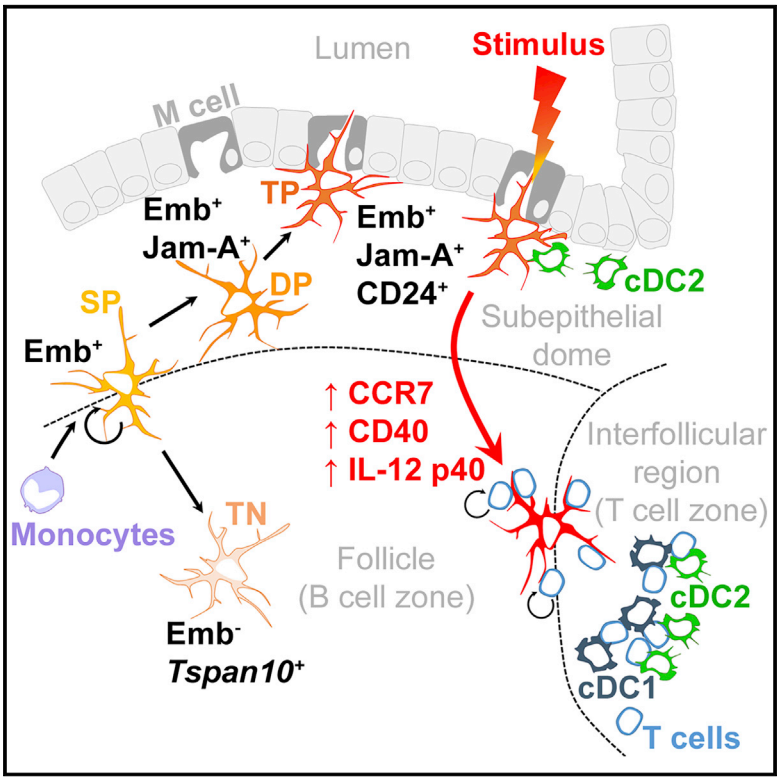

Authors

Camille Wagner, Johnny Bonnardel, Clément Da Silva, ..., Alexandre Chollat-Namy, Jean-Pierre Gorvel, Hugues Lelouard

Correspondence

lelouard@ciml.univ-mrs.fr

In Brief

Wagner et al. dissect the differentiation pathways of the Peyer's patch monocyte-derived dendritic cells termed LysoDCs. They show that LysoDCs mature as they get closer to the epithelium. Mature LysoDCs migrate to the periphery of the T cell zone, where proliferation of immune cells occurs only when stimulated.

Highlights

- Peyer's patch monocyte-derived LysoDCs follow two main differentiation pathways
- One of the two LysoDC differentiation paths leads to acquisition of DC features
- LysoDCs mature while getting closer to the epithelium
- Mature LysoDCs migrate to the periphery of the T cell zones only when stimulated

Wagner et al., 2020, Cell Reports *31*, 107479
April 7, 2020
https://doi.org/10.1016/j.celrep.2020.03.043

CellPress

Cell Reports
Article

Differentiation Paths of Peyer's Patch LysoDCs Are Linked to Sampling Site Positioning, Migration, and T Cell Priming

Camille Wagner,[1,7] Johnny Bonnardel,[1,4,5,7] Clément Da Silva,[1,6,7] Lionel Spinelli,[1] Cynthia Arroyo Portilla,[1,2] Julie Tomas,[1] Margaux Lagier,[1] Lionel Chasson,[1] Marion Masse,[1] Marc Dalod,[1] Alexandre Chollat-Namy,[3] Jean-Pierre Gorvel,[1] and Hugues Lelouard[1,8,*]

[1]Aix-Marseille Université, CNRS, INSERM, CIML, 13288 Marseille, France
[2]Departamento de Análisis Clínicos, Facultad de Microbiología, Universidad de Costa Rica, 11501-2060 San José, Costa Rica
[3]Pathological Anatomy and Cytology Laboratory, 13008 Marseille, France
[4]Present address: Department of Biomedical Molecular Biology, Ghent University, Ghent, Belgium
[5]Present address: Laboratory of Myeloid Cell Ontogeny and Functional Specialisation, VIB Center for Inflammation Research, Ghent, Belgium
[6]Present address: Immunology Section, Lund University, 221 84 Lund, Sweden
[7]These authors contributed equally
[8]Lead Contact
*Correspondence: lelouard@ciml.univ-mrs.fr
https://doi.org/10.1016/j.celrep.2020.03.043

SUMMARY

The monocyte-derived phagocytes termed LysoDCs are hallmarks of Peyer's patches, where their main function is to sample intestinal microorganisms. Here, we study their differentiation pathways in relation with their sampling, migratory, and T cell-priming abilities. Among four identified LysoDC differentiation stages displaying similar phagocytic activity, one is located in follicles, and the others reside in subepithelial domes (SED), where they proliferate and mature as they get closer to the epithelium. Mature LysoDCs but not macrophages express a gene set in common with conventional dendritic cells and prime naive helper T cells *in vitro*. At steady state, they do not migrate into naive T cell-enriched interfollicular regions (IFRs), but upon stimulation, they express the chemokine receptor CCR7 and migrate from SED to the IFR periphery, where they strongly interact with proliferative immune cells. Finally, we show that LysoDCs populate human Peyer's patches, strengthening their interest as targets for modulating intestinal immunity.

INTRODUCTION

Peyer's patches (PPs) are sentinel sites scattered along the gastrointestinal tract. They are in charge of sampling intestinal antigens, detecting pathogens, and initiating appropriate mucosal immune responses (Jung et al., 2010). They contain clustered domes formed by B cell follicles separated from each other by interfollicular regions (IFRs) enriched in T cells. The follicle-associated epithelium (FAE) contains specialized epithelial cells, called M cells, that bind and rapidly transport antigens from the lumen to the subepithelial dome (SED) enriched in phagocytes (Mabbott et al., 2013; Ohno, 2016). As M cells are a signature of the FAE, the monocyte-derived phagocytes called LysoDCs represent a hallmark of the SED (Da Silva et al., 2017). Subepithelial LysoDCs and the macrophages termed LysoMacs are the main phagocytes involved in the uptake of luminal particulate materials and pathogenic bacteria, such as *Salmonella Typhimurium* and *Listeria monocytogenes* (Bonnardel et al., 2015a; Disson et al., 2018; Lelouard et al., 2010, 2012). They are also involved in the sensing of the microbiota through expression of specific C-type lectin receptors, such as Mincle (Martinez-Lopez et al., 2019). In addition, subepithelial LysoDCs and LysoMacs display strong innate antiviral and antibacterial gene signatures and express the viral restriction factor BST2 and the antibacterial enzyme lysozyme (Bonnardel et al., 2015a; Lelouard et al., 2010). Therefore, they both represent the first PP innate immune defense barrier. They also both secrete IL-6 and TNF proinflammatory cytokines upon stimulation (Bonnardel et al., 2015a). However, unlike LysoMacs, LysoDCs display a rapid renewal rate, strongly express genes of the major histocompatibility complex class II (MHCII) presentation pathway and prime naive helper T cells for IFNγ and IL-17 production (Bonnardel et al., 2015a; Martinez-Lopez et al., 2019). Thus, LysoDCs have functional properties in common with both macrophages (e.g., phagocytosis and innate defense) and conventional dendritic cells (cDCs) (e.g., T cell priming). They actually display strong phenotypic similarities with the cDCs that express SIRPα (cDC2). However, cDC2 express or not CD11b depending on their location and differentiation state but never express high levels of the typical monocyte-derived cell markers CX_3CR1 and MerTK, which can be used to distinguish LysoDCs from cDC2 (Bonnardel et al., 2017; Da Silva et al., 2017).

Here, we studied the differentiation pathways of LysoDCs in relation to their proliferative, antigen uptake, migratory, and T cell-priming activities. We previously showed that the TLR7 agonist R848 promotes helper T cell priming by LysoDCs *in vitro* through increased interactions between both partners

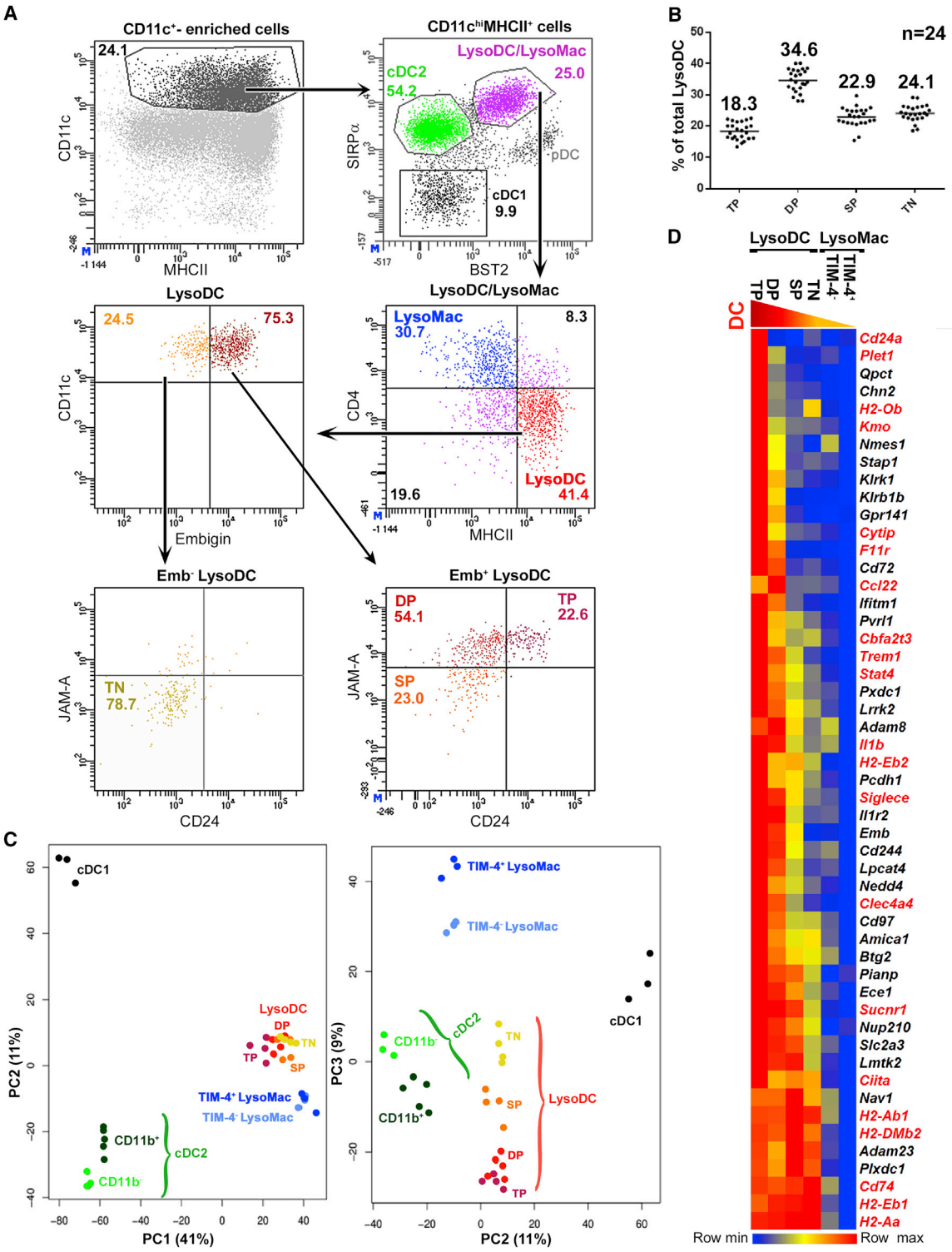

Figure 1. LysoDCs Encompass Four Subsets Showing Gradual Acquisition of a DC Gene Signature

(A) Surface expression of embigin, CD24, and JAM-A made it possible to distinguish four subsets of LysoDCs. Among PP CD11c^{+}-enriched cells, CD11c^{hi}MHCII^{+} cells were analyzed for SIRPα and BST2 expression. Monocyte-derived cells (i.e., LysoDCs and LysoMacs) were gated as SIRPα^{hi}BST2^{+} cells. Then LysoDCs and LysoMacs were separated using their CD4 and MHCII differential expression before analysis of embigin, CD24, and JAM-A expression on LysoDCs.

(B) Percentage of TP (triple positive; embigin^{+}JAM-A^{+}CD24^{+}), DP (double positive; embigin^{+}JAM-A^{+}CD24^{-}), SP (single positive; embigin^{+}JAM-A^{-}CD24^{-}), and TN (triple negative; embigin^{-}JAM-A^{-}CD24^{-}) LysoDCs was determined on 24 independent experiments with at least six mice per experiment.

(legend continued on next page)

and upregulation of LysoDC surface expression of MHCII, CD40, and CD86 (Bonnardel et al., 2015a). Thus, we next investigated the effect of R848 on the biology of LysoDCs *in vivo*. Whereas at steady state, LysoDCs reside in the SED and in the follicle but rarely in the IFR, R848 induced the expression of the key chemokine receptor CCR7 in mature LysoDCs and promoted their migration to the periphery of the IFR, where T cell activation occurred. Migratory activated LysoDCs interacted with helper T cells, among which some were proliferating. In addition, we identified and phenotypically characterized human PP LysoDCs.

RESULTS

LysoDCs Encompass Four Subsets Showing Gradual Acquisition of a DC Gene Signature

LysoDCs and LysoMacs, which are both derived from circulating monocytes, are distinguished by their differential expression of CD4 and of the MHCII molecules. We recently obtained their respective gene expression profiles (Bonnardel et al., 2015a, 2015b). *Emb* (embigin), *Cd24a* (CD24), and *F11r* (JAM-A) belonged to the LysoDC top ten upregulated genes compared with LysoMacs (Figure S1A). *Cd24a* was also expressed by all cDCs, whereas *Emb* and *F11r* were strongly expressed by CD11b$^-$ and CD11b$^+$ SIRPα^+ cDCs (cDC2) but not by SIRPα^- cDCs (cDC1) (Figure S1B). We first validated the expression of these genes at the protein level. Monocyte-derived cells were gated among CD11c^{hi}MHCII$^+$ cells on the basis of their BST2 and SIRPα expression (Figure 1A). Then LysoDCs were gated on the basis of their strong MHCII expression and lack of CD4 and were subsequently analyzed for embigin, JAM-A, and CD24 expression. Although a first subpopulation representing 24.1% ± 2.7% of total LysoDCs (n = 24) did not express embigin, JAM-A, or CD24 (triple negative [TN]), a second one (22.9% ± 3.1%; n = 24) expressed only embigin (single positive [SP]), a third one (34.6% ± 3.7%; n = 24) expressed embigin and JAM-A but not CD24 (double positive [DP]), and finally, a fourth one (18.3% ± 2.7%; n = 24) expressed all three markers (triple positive [TP]; Figures 1A and 1B).

We sorted quadruplicates of TN, SP, and TP and a quintuplicate of DP LysoDCs (see Figure S1C for gating strategy and post-sorting analysis of cell purity) to analyze their transcriptional profile using whole-mouse genome microarray (GEO: GSE133864). As expected from our previous study (Bonnardel et al., 2017), principal-component analysis separated monocyte-derived from common DC precursor-derived cells and SIRPα^+ (cDC2, LysoDCs, and LysoMacs) from SIRPα^- (cDC1) phagocytes (Figure 1C). According to the third principal component, TN and TP LysoDCs appeared at the two extremes of a transcriptional continuum integrating SP and DP LysoDCs as intermediates (Figure 1C). We recently defined a list of 51 genes that are expressed by PP cDC2 and LysoDCs but not by LysoMacs (Bonnardel et al., 2015a). There was a gradual increase in the expression of this LysoDC and cDC2 common list of genes from TN to TP LysoDCs (Figure 1D). Actually, TP LysoDCs expressed the full list of genes, whereas TN expressed less than half of it (Figure 1D). In summary, LysoDCs comprise four subsets characterized by the progressive acquisition of a DC gene signature.

Single-Cell RNA-Sequencing Reveals LysoDC Transcriptional Plasticity and Dynamics of Differentiation

To deepen our knowledge of LysoDC subsets, we next performed single-cell RNA sequencing of LysoDCs (GEO: GSE141776). Through a t-stochastic neighbor embedding (t-SNE) analysis (Amir et al., 2013; van der Maaten and Hinton, 2008), we identified two main groups of cells (Figure 2A). The minor group represented about 10% of LysoDCs (Figure 2A, clusters 1 and 2), most of which expressing *Emb* but not *F11r* or *Cd24a* (SP LysoDCs; Figure 2B). These SP LysoDCs displayed a strong cell cycle signature and partitioned into two clusters corresponding to the G1/S (cluster 1; *Mcm6* and *Ccne1* expression) and G2/M (cluster 2; *Cenpa* and *Ccnb2* expression) phases of the cell cycle (Figure 2B). These data suggest that SP LysoDCs are actively replicating and are the main precursor of LysoDCs.

The non-proliferative group of LysoDCs partitioned into four clusters (clusters 3–6; Figure 2A). Cluster 3, like clusters 1 and 2, contained mainly *Emb*$^+$*F11r*$^-$*Cd24*$^-$ SP LysoDCs (Figure 2B) and showed strong *Actb* expression, suggesting that SP LysoDCs undergo cytoskeleton rearrangement to initiate their maturation program and/or increase their motility and antigen uptake ability (Figure 2B). *Il1b* has been shown to be the main cytokine gene enriched in LysoDCs and cDC2 compared with LysoMacs (Bonnardel et al., 2015a: Figure S2A). As its expression increased from cluster 3 to cluster 4 to reach its peak in cluster 5 (Figures 2B and S2B), it suggests a path of LysoDC maturation from cluster 3 to cluster 5. Cluster 4, like cluster 3, contained *Emb*$^+$*F11r*$^-$*Cd24*$^-$ SP LysoDCs but also *Emb*$^+$*F11r*$^+$*Cd24*$^-$ DP LysoDCs (Figure 2B), thus strengthening the hypothesis that cluster 3 gave rise to cluster 4. Genes expressed mainly by TP LysoDCs and cDC2 (i.e., *Plet1* and *Cd24a*) (Figures 1D and S2A) were found in cluster 5, especially at its border with clusters 3 and 4 (Figure 2B). However, *Plet1*, *Cd24a*, and even *Emb* expression decreased in the distal region of cluster 5, unlike that of *Clec4d*, which increased (Figure 2B). *Clec4d* expression upregulation by TP but also DP LysoDCs compared with SP and TN LysoDCs was confirmed by our microarray data (Figure S2A). *Cd9* and *Ifitm1*, whose expression was restricted mainly to DP and TP LysoDCs (Figure S2A),

(C) Principal-component analysis of PP phagocytes is shown. The first (PC1) and second (PC2) principal components separated cDCs (cDC1 and cDC2) from monocyte-derived cells (LysoMacs and LysoDCs) and SIRPα^- (cDC1) from SIRPα^+ (cDC2, LysoDCs, and LysoMacs) phagocytes, respectively. The third principal component (PC3) showed a transcriptional continuum of LysoDC subsets ranging from TN to TP, with SP and DP as intermediates.
(D) Heatmap of the list of 51 genes that are expressed by PP cDC2 and LysoDCs but not by LysoMacs, which express or not TIM-4 depending on their location in the IFR or in the SED, respectively (Bonnardel et al., 2015a). Expression of this list of genes progressively increased from TN to TP subset. Genes known to be involved in DC functions are in red.
See also Figure S1.

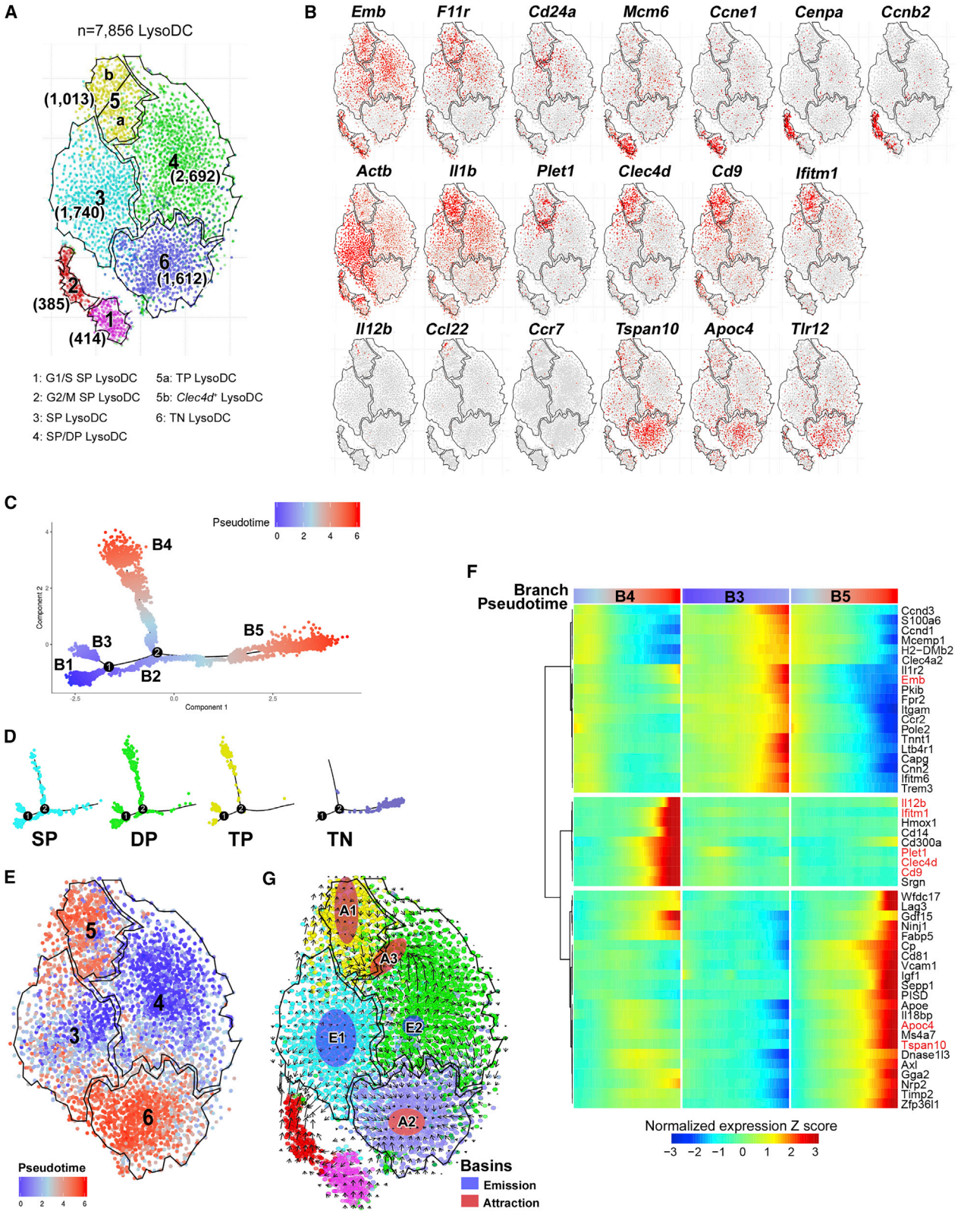

(legend on next page)

were expressed in the whole of cluster 5, indicating that they were key markers of the latter (Figures 2B and S2B). *Il12b*, *Ccl22*, and *Ccr7*, which are known to be expressed by activated cDCs (Dieu et al., 1998; Förster et al., 1999; Macatonia et al., 1995; Tang and Cyster, 1999), were expressed by very few cells of the distal region of cluster 5 (Figures 2B and S2B). Finally, cluster 6 corresponded to TN LysoDCs with no *Emb*, *F11r*, or *Cd24a* expression (Figure 2B). *Tspan10*, *Tlr12*, and *Apoc4* were major discriminating genes of cluster 6 (Figures 2B and S2B). Their expression by TN LysoDCs was confirmed by our microarray data (Figure S2A).

To detail LysoDC differentiation pathway(s), we used Monocle 2, an algorithm that reveals complex single-cell trajectories and multiple cell fate decisions through pseudotemporal ordering of single cells along a spanning tree (Qiu et al., 2017). Monocle 2 resolved non-proliferative LysoDCs (clusters 1 and 2 were excluded from the analysis) into three main trajectory branches, in which one had a sub-branching (Figures 2C and S2C). SP LysoDCs were the main subset between fate decision nodes 1 and 2, consistent with our hypothesis defining them as precursors (Figures 2D and S2C). Taking the branch tip that contains the largest number of SP LysoDCs (B1; Figure S2C) as root for pseudotime analysis clearly identified DP/TP (B4; t-SNE cluster 5) and TN (B5; t-SNE cluster 6) LysoDCs as differentiation endpoints (Figures 2C and 2E). Differentially expressed genes in pseudotime across branches included t-SNE cluster-defining genes and revealed coordinated gene expression profiles defining the differentiation paths of LysoDCs (Figure 2F).

To strengthen these findings and determine without any supervision the precursors and products among LysoDCs, we used a recently published method of mRNA velocity estimation based on the ratio between spliced and unspliced mRNA levels (La Manno et al., 2018). This method predicts trajectories of cell differentiation in pseudotime through visualization of a vector field. The projection of the velocity vector field onto the t-SNE map showed the main zones of differentiation departure (emission basins) and endpoint (attraction basins) (Figure 2G). LysoDCs strongly diverged at the level of restricted area of clusters 3 and 4 (Figure 2G, emission basins) to give rise to other clusters. Cluster 5 and cluster 6 but also the border between clusters 4 and 5 were endpoints of LysoDC differentiation (Figure 2G, attraction basins). There was good correspondence between RNA velocity emission/attraction basins and Monocle 2 branch trajectories (Figures 2E, 2G, and S2D). In summary, RNA velocity not only confirmed that SP LysoDCs are the precursors of LysoDCs and TN and TP their two main terminal differentiation stages but revealed the fate trajectories and multiple decision choices of LysoDCs.

LysoDCs Are Located Mainly in the SED Except for TN LysoDCs Located in the Follicle

To locate immature LysoDCs (SP LysoDCs) that proliferate in PP (Figure 2A, clusters 1 and 2), we looked at Ki-67 expression by microscopy. We indeed detected Ki-67 in the nuclei of some embigin-expressing LysoDCs (CX_3CR1^+ $CD11c^+$ $CD4^-$ cells) in the SED, one of which was caught in the process of nuclear division (Figure 3A; Video S1).

Most subepithelial LysoDCs expressed embigin, whereas follicular LysoDCs did not, indicating that SP, DP, and TP LysoDCs were located mainly in SED, whereas TN LysoDCs were in follicles (Figures 3B and 3C). Expression of the chemokine receptor CXCR5 is known to be required for migration of B cells and follicular helper T cells to the follicles (Ansel et al., 2000; Breitfeld et al., 2000; Förster et al., 1996; Gunn et al., 1998; Legler et al., 1998; Schaerli et al., 2000). We thus investigated whether CXCR5 was involved in TN LysoDC location. *Cxcr5* was not detected above background in the gene expression database of PP phagocytes (Figure S3A). Moreover, when we reconstituted lethally irradiated mice with a 1:1 mixture of bone marrow cells isolated from CX3CR1-$GFP^{-/+}$ mice and CXCR5-deficient mice, both GFP^+ (originating from the CXCR5-proficient mice) and GFP^- (originating from the CXCR5-deficient mice) monocyte-derived cells were able to reach the follicles (Figure S3B). Therefore, location of TN LysoDCs in follicles is likely independent of CXCR5.

JAM-A expression by subepithelial LysoDCs was detected from the base to the top of the dome, but its expression increased while getting closer to the epithelium (Figures 3D, S3C, and S3D). Finally, CD24 was expressed by too many immune cells to clearly establish the location of $CD24^+$ and $CD24^-$ LysoDCs (Figure S3E). We therefore decided to use PLET1 (Depreter et al., 2008) as a marker of TP LysoDCs, as it

Figure 2. Single-Cell RNA Sequencing Reveals LysoDC Transcriptional Plasticity and Dynamics of Differentiation

(A–G) Single-cell mRNA sequence analysis of 7,856 LysoDCs.

(A) t-Stochastic neighbor embedding (t-SNE) map colored by Seurat clustering showed two groups of 799 and 7,057 LysoDCs partitioned into two and four clusters, respectively. Numbers of cells per cluster are in brackets.

(B) Expression of selected genes on t-SNE map allowed the identification of cells from cluster 1 as SP LysoDCs in G1/S mitotic phase (*Emb*$^+$*F11r*$^-$*Cd24a*$^-$*Mcm6*$^+$*Ccne1*$^+$), from cluster 2 as SP LysoDCs in G2/M mitotic phase (*Emb*$^+$*F11r*$^-$*Cd24a*$^-$*Cenpa*$^+$*Ccnb2*$^+$), from cluster 3 as SP LysoDCs (*Emb*$^+$*F11r*$^-$*Cd24a*$^-$), from cluster 4 as SP and DP LysoDCs (*Emb*$^+$*F11r*$^-$*Cd24a*$^-$ and *Emb*$^+$*F11r*$^+$*Cd24a*$^-$, respectively), from cluster 5 as TP LysoDCs (*Emb*$^+$*F11r*$^+$*Cd24a*$^+$*Plet1*$^+$; cluster 5a) and *Clec4d*$^+$ LysoDCs (cluster 5b), and from cluster 6 as TN LysoDCs (*Emb*$^-$*F11r*$^-$*Cd24a*$^-$*Tspan10*$^+$).

(C–F) Monocle 2 pseudotime analysis of LysoDC.

(C) Monocle 2 spanning tree.

(D) Projection of TN, SP, DP, and TP LysoDCs onto the Monocle 2 spanning tree shown in (C).

(E) Projection of the pseudotime analysis onto the t-SNE clustering shown in (A).

(F) Heatmap of top 50 differentially expressed genes in pseudotime across B3, B4, and B5 branches of Monocle 2 trajectories. The t-SNE cluster-defining genes are in red.

(G) RNA velocity analysis projected onto the t-SNE clustering showing the extrapolated future states of cells (arrows) on the basis of their unspliced versus spliced mRNA ratio. The RNA velocity vector field allowed the identification of two emission basins of differentiation (E1 and E2; blue area of clusters 3 and 4) and three differentiation endpoints (A1, A2, and A3; red area of cluster 5, cluster 6, and the border between clusters 4 and 5, respectively).

See also Figure S2.

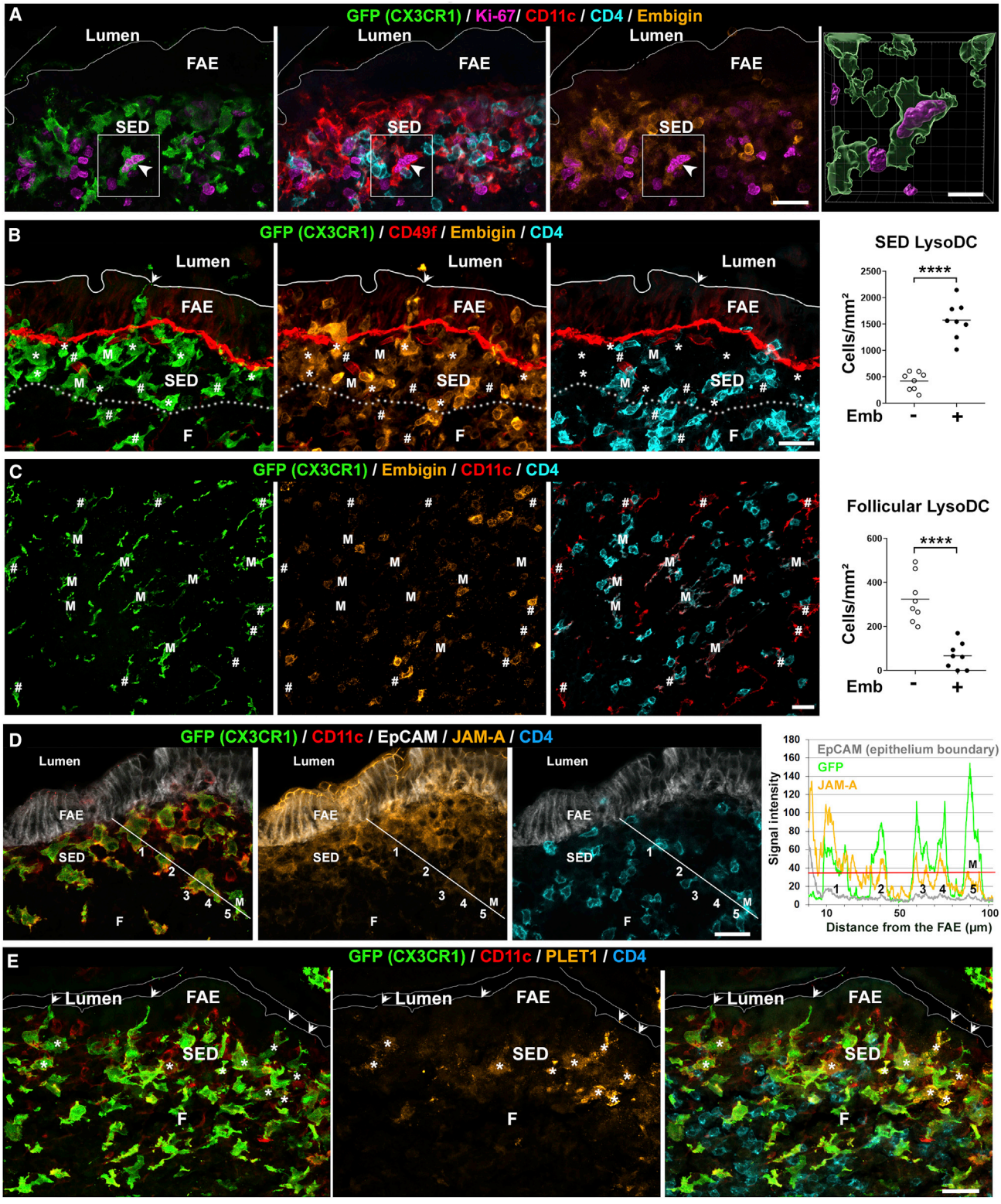

(legend on next page)

was their second most upregulated gene within the LysoDC population after *Cd24a* (Figures 1D, 2B, and S2A). In contrast to CD24, the only cells that expressed PLET1 were a few cDC2 and LysoDCs close to the FAE, as well as some LysoDCs extending trans-M cell dendrites (Figure 3E).

In summary, TN LysoDCs are scattered through the upper part of the follicle, whereas other LysoDCs are located mainly in the SED, with DP and TP LysoDCs (JAM-A$^+$ LysoDCs) being closer to the epithelium than SP LysoDCs.

Human PP Encompass a Population of Subepithelial Cells Phenotypically Related to LysoDCs

We previously showed that some human PP subepithelial cells express lysozyme (Lelouard et al., 2010), and we next decided to investigate their phenotype. In mouse, LysoMacs are distinct from villous macrophages and have been shown to express or not the apoptotic receptor TIM-4 depending on their location in the IFR or SED, respectively (Wagner et al., 2018). Similarly, human PP macrophages displayed a distinct phenotype from that of their villus counterparts, as illustrated by the lack of CD163 and TIM-4 expression in the SED and in the upper part of the follicle (Figures S4A and S4B). However, at the base of the follicle and in the IFR, macrophages expressed CD163 and TIM-4 (Figure S4B). Moreover, Tingible-body macrophages of the germinal center expressed TIM-4 but not CD163 (Figure S4C).

Human subepithelial lysozyme-expressing cells strongly expressed CD11c and SIRPα but were negative for CD1c, a marker of human cDC2 (Figure 4A). The main markers that distinguish mouse LysoDCs from LysoMacs are CD4, MHCII, and the LysoDC maturation markers embigin, JAM-A, and CD24 (Bonnardel et al., 2015a). In contrast to mice, CD4 expression was observed in all human subepithelial lysozyme-expressing cells and could not be used to separate LysoDCs from LysoMacs (Figure S4D). Nevertheless, most human subepithelial CD11c$^+$ SIRPα^+ lysozyme-expressing cells expressed strong levels of MHCII (Figure 4B). Some also expressed the markers of LysoDC maturation JAM-A and CD24 (Figures 4C and 4D). Interestingly, some of these cells resided in the FAE or extended dendrites into it to reach the gut lumen, suggesting a role in intestinal antigen sampling similar to mouse LysoDCs (Figures 4A–4C). Finally, a few of them expressed Ki-67, suggesting that they may have the potential to proliferate (Figure 4E). In summary, we identified human PP subepithelial phagocytes that are phenotypically related to mouse LysoDCs.

R848 Stimulation Promotes Activation of LysoDCs but Does Not Block Their Phagocytic Ability

As LysoDCs are the main phagocytic cells of the SED (Bonnardel et al., 2015a; Lelouard et al., 2010, 2012), we investigated particulate antigen uptake ability of LysoDC maturation states. They all efficiently internalized 0.5 μm microspheres *in vitro*, whereas PP cDC2 were poorly phagocytic (Figures 5A and 5B). Because DCs are believed to stop antigen uptake when stimulated (Mellman and Steinman, 2001), we investigated whether LysoDC ability for phagocytosis was altered upon TLR stimulation. In PP, LysoDCs and pDCs but no other phagocytes express TLR7 (Bonnardel et al., 2017). *Tlr7* was expressed independently of LysoDC maturation states (Figure S5A). When stimulated with the TLR7 ligand R848, LysoDCs continued to engulf microspheres, although their efficiency decreased (Figures 5C–5E).

To better appreciate the impact of R848 treatment on LysoDCs *in vivo*, we examined the number of each LysoDCs subset in PP from mice fed or not with R848 and noted transient increases of both DP and TP LysoDC numbers (Figure S5B). We next analyzed the transcriptional changes induced by R848 treatment on DP and TP LysoDC subsets using whole-mouse genome microarray and compared them with those of TIM-4$^-$ and TIM-4$^+$ LysoMacs and cDCs. Hierarchical clustering showed that, unlike activated cDCs, which cluster together apart from their resting counterparts whatever subset they belong to (Bonnardel et al., 2017), activated LysoDCs clustered with resting LysoDCs apart from activated LysoMacs, which clustered with resting LysoMacs (Figure S5C). Thus, LysoDCs conserved their transcriptional specificity upon activation. A set of 60 genes was upregulated in TP LysoDCs upon R848 stimulation (Figure S5D), which is very few compared to what is

Figure 3. LysoDCs Are Mainly in the SED, Except for TN LysoDCs, Located in the Follicle

(A–E) Spectral confocal imaging projection of PP tissue sections from CX3CR1-GFP$^{-/+}$ mice.

(A) The PP section was stained for GFP (green), Ki-67 (magenta), CD11c (red), CD4 (cyan), and embigin (orange). Subepithelial embigin-positive LysoDC (CX$_3$CR1$^+$ CD11c$^+$ CD4$^-$ cells) expressing Ki-67 in its nucleus (arrowhead). The three-dimensional reconstruction of the boxed area shows the nuclear division inside the LysoDC.

(B) Left: PP section stained for GFP (green), CD49f (red), embigin (orange), and CD4 (cyan). Embigin-positive (asterisks) but not embigin-negative (hashes) LysoDCs (CX$_3$CR1$^+$ CD4$^-$ cells) were enriched in the SED, delineated by a dotted line. Some embigin-positive LysoDCs extended dendrites into the lumen (arrowhead) or penetrated the FAE, delineated by CD49f (basal lamina staining). Note that helper T cells (small CD4$^+$ cells) expressed embigin as well. M, LysoMacs (CX$_3$CR1$^+$CD4$^+$ cells). Right: quantification of embigin-positive and negative LysoDCs in the SED of PP from three CX3CR1-GFP$^{-/+}$ mice issued from different breeding (two or three tissue sections per mouse). ****$p < 0.0001$, unpaired t test with Welch's correction.

(C) Left: PP follicle section stained for GFP (green), CD11c (red), embigin (orange), and CD4 (cyan). Embigin-negative (hashes) but not embigin-positive (asterisks) LysoDCs (CX$_3$CR1$^+$ CD4$^-$ cells) were enriched in the follicle. M, LysoMacs (CX$_3$CR1$^+$CD4$^+$ cells). Right: quantification of embigin-positive and negative LysoDCs in the follicle of PP from three CX3CR1-GFP$^{-/+}$ mice issued from different breeding (one to three tissue sections per mouse). ****$p < 0.0001$, unpaired t test with Welch's correction.

(D) Left: subepithelial LysoDCs (CX$_3$CR1$^+$CD11c$^+$CD4$^-$ cells) close to the FAE labeled with EpCAM (gray) expressed JAM-A (orange). Right: quantification of GFP (green) and JAM-A (orange) intensity signals along the white line of the left image showing decreased JAM-A expression with increased distance from the FAE. The red line indicates the level of autofluorescence displayed by a LysoMac (CX$_3$CR1$^+$CD11c$^+$CD4$^+$ cell 5, M) in the JAM-A channel.

(E) A few LysoDCs (CX$_3$CR1$^+$CD11c$^+$CD4$^-$ cells) and cDC2 (CX$_3$CR1$^-$CD11c$^+$) close to the FAE expressed PLET1 (asterisk). Some LysoDCs extended dendrites into the FAE to reach the gut lumen (arrowheads), among which one expressed PLET1 (asterisk).

Bars, 20 μm with the exception of the reconstruction in (A), 10 μm. Pictures are representative of at least three independent experiments.

See also Figure S3 and Video S1.

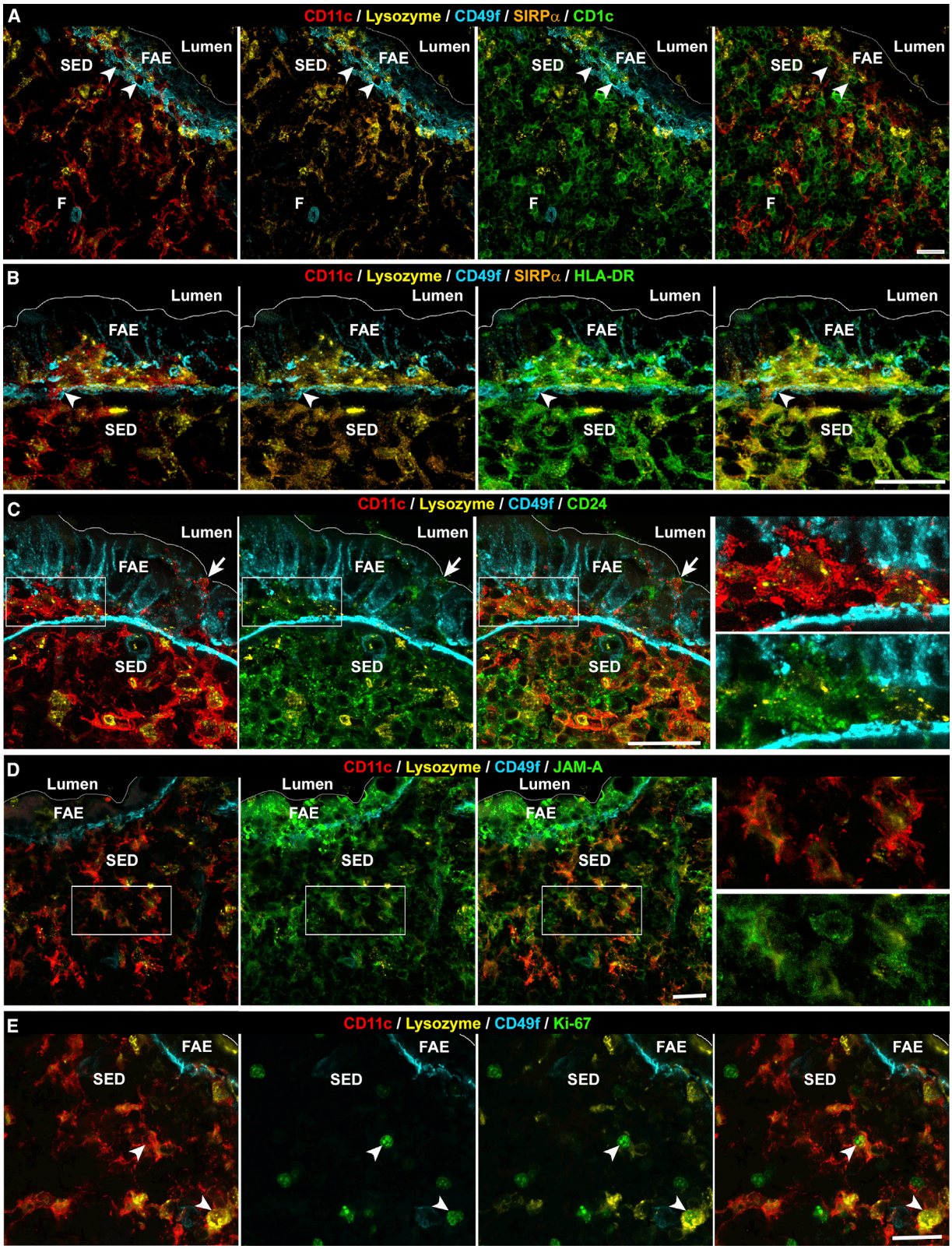

(legend on next page)

observed for dome cDC1 (483 genes) and cDC2 (210 genes) (Bonnardel et al., 2017). Interestingly, *Il12b*, *Ccl22*, and *Ccr7*, which were all expressed at steady state by very few TP LysoDCs (Figure 2B), belonged to these 60 genes (Figure S5D), strengthening the assumption that TP LysoDCs correspond to the most mature LysoDCs.

Subepithelial Mature LysoDCs Upregulate CCR7 and Migrate to the Periphery of the IFR upon R848 Stimulation

Upon *in vivo* R848 stimulation, *Ccr7* was upregulated in TP LysoDCs, whereas genes related to the developmental pathway of cDCs, such as *Zbtb46* and *Flt3*, were not (Figure S5D). At steady state, LysoDCs are located mainly in the SED and scattered throughout the follicle but rarely present in the IFR (Bonnardel et al., 2015a, 2017). Upregulation of *Ccr7* in TP LysoDCs upon R848 stimulation could lead to their migration in the IFR in a similar way as do cDCs (Bonnardel et al., 2017; Iwasaki and Kelsall, 2000). We next checked whether subepithelial LysoDCs really expressed CCR7 upon stimulation. At steady state, we failed to detect any CCR7 expression in the SED (Figure 6A). However, only 4 h after R848 gavage, we observed strong CCR7 expression at the surface and in intracellular compartments of subepithelial cDCs ($CD11c^+CX_3CR1^-CD4^-$ cells; Figure 6B). Then, a second burst of CCR7 expression occurred in the SED at 8 h post-R848 gavage, but this time CCR7 expression was confined mainly to LysoDCs ($CD11c^+CX_3CR1^+CD4^-$ cells; Figure 6C). Although some LysoMacs ($CD11c^+CX_3CR1^+CD4^+$ cells) were in close contact with CCR7-expressing LysoDCs, they never expressed CCR7 (Figure 6C). At the same time, $CCR7^+$ LysoDCs were observed at the periphery of the IFR, suggesting that they could have migrated from the SED to the IFR periphery (Figure 6D). Interestingly, CCR7 was located mainly in intracellular compartments of subepithelial LysoDCs, whereas it was expressed at the surface of LysoDCs that had already left the SED, suggesting that their migration occurred only upon CCR7 cell surface expression (Figures 6C and 6D, insets). Importantly, 16 h after R848 treatment, the increased number of LysoDCs at the IFR periphery was consistent with their decreased number in the SED (391 ± 125 fewer LysoDCs per square millimeter in the SED versus 407 ± 90 more LysoDCs per square millimeter at the IFR periphery; Figures 6E and S6A). Altogether, these data suggest that upon R848 treatment, mature LysoDCs express CCR7 and migrate from the SED to the IFR periphery but with a delay compared with cDCs.

Mature LysoDCs Efficiently Prime Naive Helper T Cells *In Vitro* and Strongly Interact with Them at the Site of Their Proliferation upon Stimulation *In Vivo*

R848 induces an indirect TNF-dependent activation of all cDC subsets (Bonnardel et al., 2017; Yrlid et al., 2006). All interfollicular cDC1 and R848-activated cDC2 express the C-type lectin receptor CD205 (Bonnardel et al., 2017). In addition, R848-activated cDC2 that migrate from the dome-associated villi to the IFR express the type I transmembrane glycoprotein CD101 (Bonnardel et al., 2017). Finally, all PP R848-activated cDCs express high levels of CCR7 (Bonnardel et al., 2017). CD205, CD101, and CCR7 were indeed strongly expressed in the IFR of 16 h R848-treated mice but not at the IFR periphery (Figures 7A, S6B, and S6C). Therefore, upon R848 treatment, there was a clear temporal and spatial segregation between activated cDCs and LysoDCs, the latter accumulating at the IFR periphery (i.e., the transition area between the B and the T cell zones).

Interestingly, many immune cells, including helper T cells, were proliferating in this region (Figures 7A, 7B, and S6), suggesting that the IFR periphery is likely a preferential site of T cell activation and proliferation. Moreover, LysoDCs were strongly interacting with helper T cells, some of which were engaged in division (Figures 7C and 7D; Figures 7A, S6B, and S6C, insets). The plasma membrane of LysoDCs surrounded large surfaces of proliferating T cells, suggesting a tight and likely long-lasting interaction between both partners (Figure 7C; Video S2).

Upon R848 stimulation, *Il12b* expression was upregulated in stimulated TP and DP LysoDCs but not in cDCs (Figure S5D). We investigated the expression of IL-12 p40 in PP using a transgenic mouse model in which eYFP is expressed upon IL-12 p40 production (Reinhardt et al., 2006). Following stimulation with R848, eYFP was indeed strongly induced in LysoDCs and LysoMacs but not or weakly in cDCs (Figure S7A). In this mouse model, MerTK was used to label monocyte-derived cells (i.e., LysoDCs and LysoMacs) because its expression was highly correlated with CX_3CR1 expression and was never found in PP cDCs (Figures S7B and S7C). At the IFR periphery, LysoDCs strongly expressed eYFP upon R848 stimulation, as demonstrated by MerTK expression of most eYFP-expressing cells (Figure 7E). IL-12 p40-expressing LysoDCs were in tight interaction with helper T cells, some of which were proliferating (Figure 7E). Moreover, interfollicular but not subepithelial LysoDCs expressed the key costimulatory molecule CD40, which was enriched at the site of interaction with proliferating helper T cells (Figure 7F). Some proliferative T cells strongly interacting with LysoDCs displayed high levels of CD69, confirming T cell early-activated status (Figure 7G).

Finally, to determine whether mature TP LysoDCs could better prime naive helper T cells than immature LysoDCs, all subsets were isolated, loaded with ovalbumin, and incubated with ovalbumin-specific naive helper T cells 4 days before monitoring the proliferation of the latter. Without any stimulation, only TP LysoDCs were able to efficiently prime naive helper T cells (Figure 7H). Altogether, these results suggest that activated mature TP LysoDCs could play a role in helper T cell priming at the periphery of the IFR.

Figure 4. Human PP Encompass a Population of Cells Phenotypically Related to LysoDCs

(A–E) Spectral confocal imaging projections of human PP sections stained for CD11c (red), lysozyme (yellow), CD49f (cyan), SIRPα (orange), and CD1c (A) or HLA-DR (B) or CD24 (C) or JAM-A (D) or Ki-67 (E) in green. (A–D) As in mouse, human PP subepithelial phagocytes expressed lysozyme, CD11c, SIRPα, and MHCII. Some of them also expressed JAM-A and CD24 but never CD1c. Some human LysoDCs could penetrate the FAE (arrowheads) and extend dendrites into the lumen (arrow). (E) Some human subepithelial LysoDCs expressed Ki-67 (arrowheads).

Bars, 20 μm. Pictures are representative of three human samples. See also Figure S4.

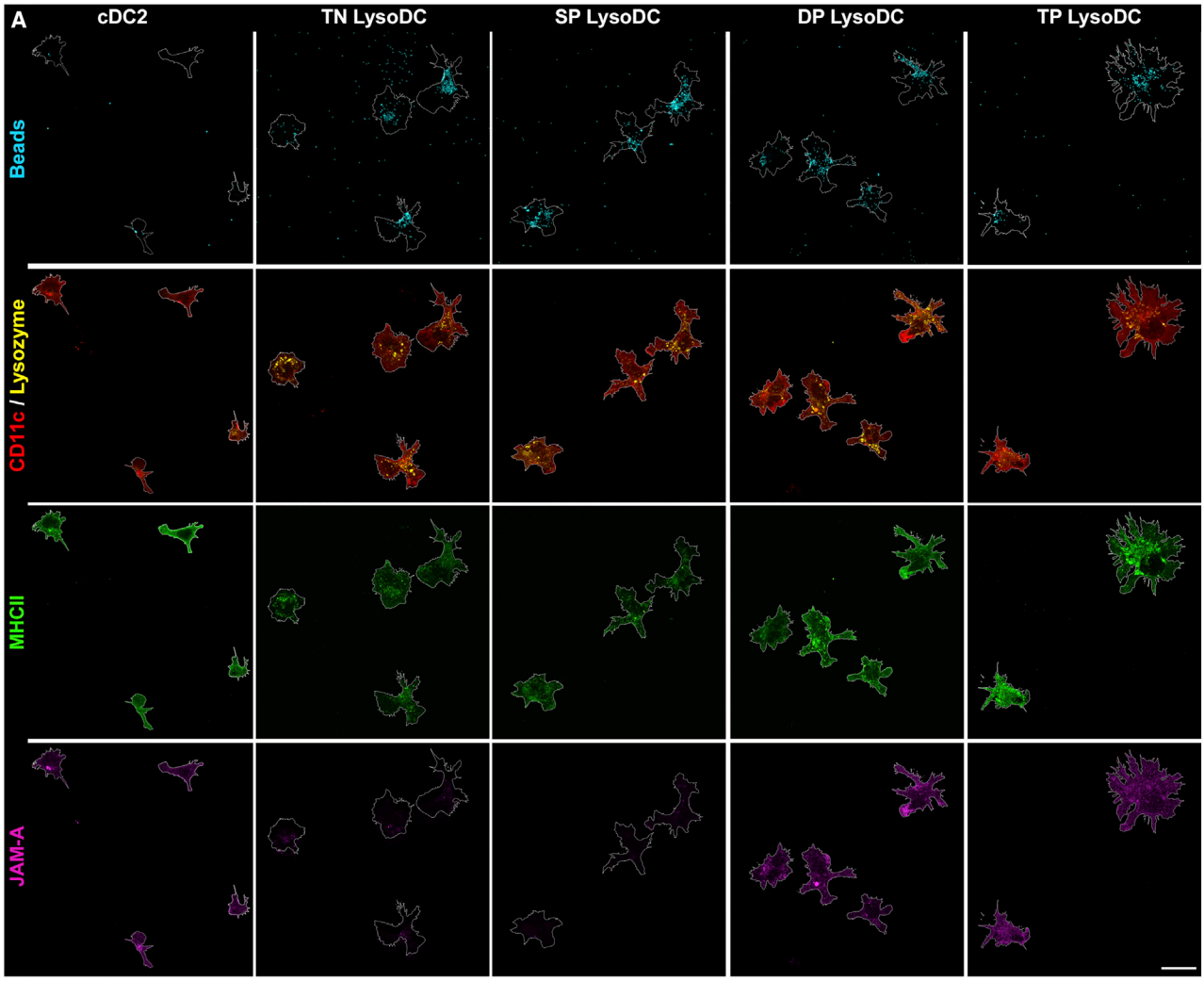

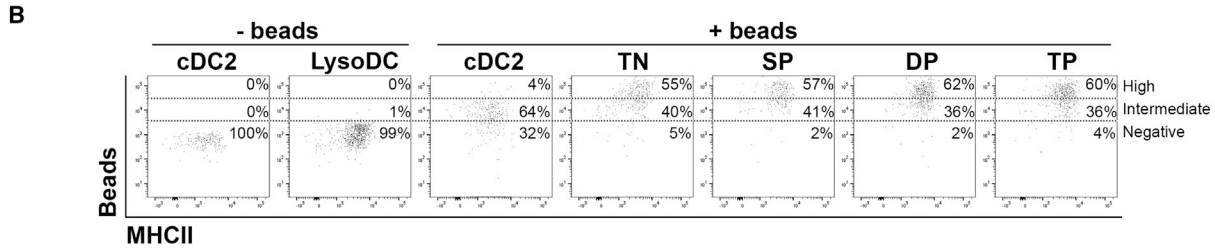

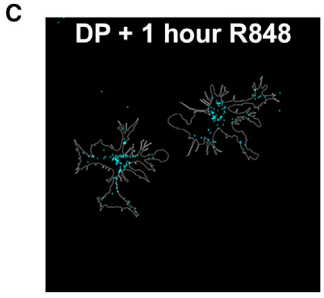

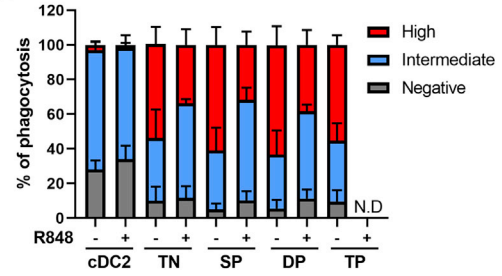

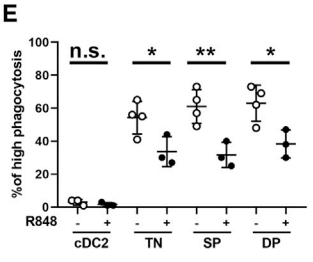

(legend on next page)

DISCUSSION

In this study, we dissected the differentiation pathways of LysoDCs in relation to their transcriptional profile, their location, and their functions. TN LysoDCs are the only LysoDCs that do not express embigin and that reside in the follicles. Therefore, they represent a distinct branch from the main LysoDC differentiation stream and may be influenced by follicular rather than subepithelial microenvironment. Although highly phagocytic as the other LysoDCs, their immune function is likely distinct from that of classic DCs, as TN LysoDCs never acquire the list of genes shared by cDC2 and TP LysoDCs. Their location rather suggests a potential role in providing support for B cells.

The TP LysoDC gene signature seems to correspond to the minimal requirement to exert DC functions, whatever the ontogeny of cells. It indeed includes antigen presentation-related genes such as MHCII-encoding genes as well as genes involved in cDC trafficking, such as *Plet1* and *F11r* (Cera et al., 2004; Karrich et al., 2019; Murakami et al., 2010). Moreover, only TP LysoDCs are able to efficiently prime naive T cells, underlying the importance of the few genes that distinguish DP from TP LysoDCs in this specific function. Nevertheless, most TP LysoDCs lack expression of crucial molecules normally expressed by activated cDCs, such as CCR7, CCL22, and IL-12 p40, which are involved in migration to T cell zones and in attraction and polarization of T cells, respectively (Dieu et al., 1998; Förster et al., 1999; Macatonia et al., 1995; Tang and Cyster, 1999). Accordingly, at steady state, LysoDCs do not migrate in the IFR to encounter naive T cells (Bonnardel et al., 2015a, 2017). They require additional signals, such as those provided by TLR ligands, to undergo an activation process that leads to their migration from the SED to the peripheral region of IFR, where proliferation of helper T cells preferentially occurs. In the absence of such signal, they may be unable to mount an adaptive immune response. This could help protect the body from unwanted and/or excessive inflammation while maintaining the possibility of responding to important threats.

We identified coordinated profiles of gene expression as well as key markers that characterize each LysoDC differentiation stage. Interestingly, some of these markers are also implicated in the differentiation/homeostatic maturation of PP cDC2 (Bonnardel et al., 2017). Thus, JAM-A expression increases during the differentiation process of both cDC2 and LysoDCs. Although its precise role remains to be established, it is already known to be involved in regulating DC trafficking (Cera et al., 2004; Murakami et al., 2010).

SP LysoDCs are likely the precursors of all other LysoDC subsets, although definitive proof has yet to be provided. Interestingly, they are able to proliferate, indicating that, in addition to replenishment by CCR2-dependent monocytes (Bonnardel et al., 2015a), LysoDCs can renew themselves. We showed that human LysoDCs likely have a similar ability to proliferate *in situ*. Moreover, on the basis of JAM-A and CD24 expression, we can hypothesize that human LysoDCs follow a differentiation pathway similar to that of their mouse counterparts. Finally, the ability of human LysoDCs to interact with the FAE and to extend dendrites reaching the gut lumen strongly supports their role in intestinal antigen sampling.

In summary, our study characterizes the differentiation pathways of LysoDCs and highlights their plasticity. However, future studies involving innovative fate-mapping transgenic mouse models, such as the one recently generated by Ginhoux and colleagues (Liu et al., 2019), will be required to provide direct evidence of precursor-product relationships between LysoDC subsets. Moreover, a specific depletion model will be necessary to fully address the role of LysoDCs in T cell priming *in vivo*. Overall, the discovery of several LysoDC outcomes paves the way of a better understanding of LysoDC functions in intestinal immunity. Moreover, the possibility of promoting their maturation and inducing their migration through stimulation at a defined time after delivery of an oral antigen opens up new opportunities to promote appropriate mucosal immune response to specific antigens.

STAR★METHODS

Detailed methods are provided in the online version of this paper and include the following:

- KEY RESOURCES TABLE
- LEAD CONTACT AND MATERIALS AVAILABILITY
- EXPERIMENTAL MODEL AND SUBJECT DETAILS
- METHOD DETAILS
  - R848 treatment
  - Antibodies

Figure 5. Phagocytic Ability of LysoDC Subsets

(A–E) PP phagocytes were sorted as shown in Figure S1C. Each sorted LysoDC subset and CD11b$^+$ cDC2 were stimulated (C–E) or not (A and B) with R848 for 1 h before adding 0.5 μm Brilliant Blue fluorescent microspheres for an additional hour.

(A) Spectral confocal imaging of microsphere uptake (cyan) by PP phagocyte subsets (delimited by a white contour in all panels to visualize bound versus internalized microspheres) stained for MHCII (green), CD11c (red), lysozyme (yellow), and JAM-A (magenta) as indicated. Cells are shown with the same magnification (bar, 20 μm). Note the smaller size and inability to capture microspheres of cDC2 compared with LysoDC subsets.

(B) Flow cytometry analysis of microsphere binding and uptake by PP phagocyte subsets.

(C) Uptake of microspheres (cyan) by DP LysoDCs (white contour) 1 h after R848 stimulation.

(D and E) Flow cytometry quantification of microsphere binding and uptake by the different phagocyte subsets.

(D) Percentage of phagocytosis with or without R848 stimulation.

(E) Percentage of highly phagocytic cells with or without R848 teatment. R848 treatment reduced but did not abrogate uptake ability of LysoDC subsets.

Data are from three (with R848) or four (without R848) independent experiments with pooled cells from 35 mice per experiment (ns, non-significant; *$p < 0.05$ and **$p < 0.01$, unpaired t test with Welch's correction).

See also Figure S5.

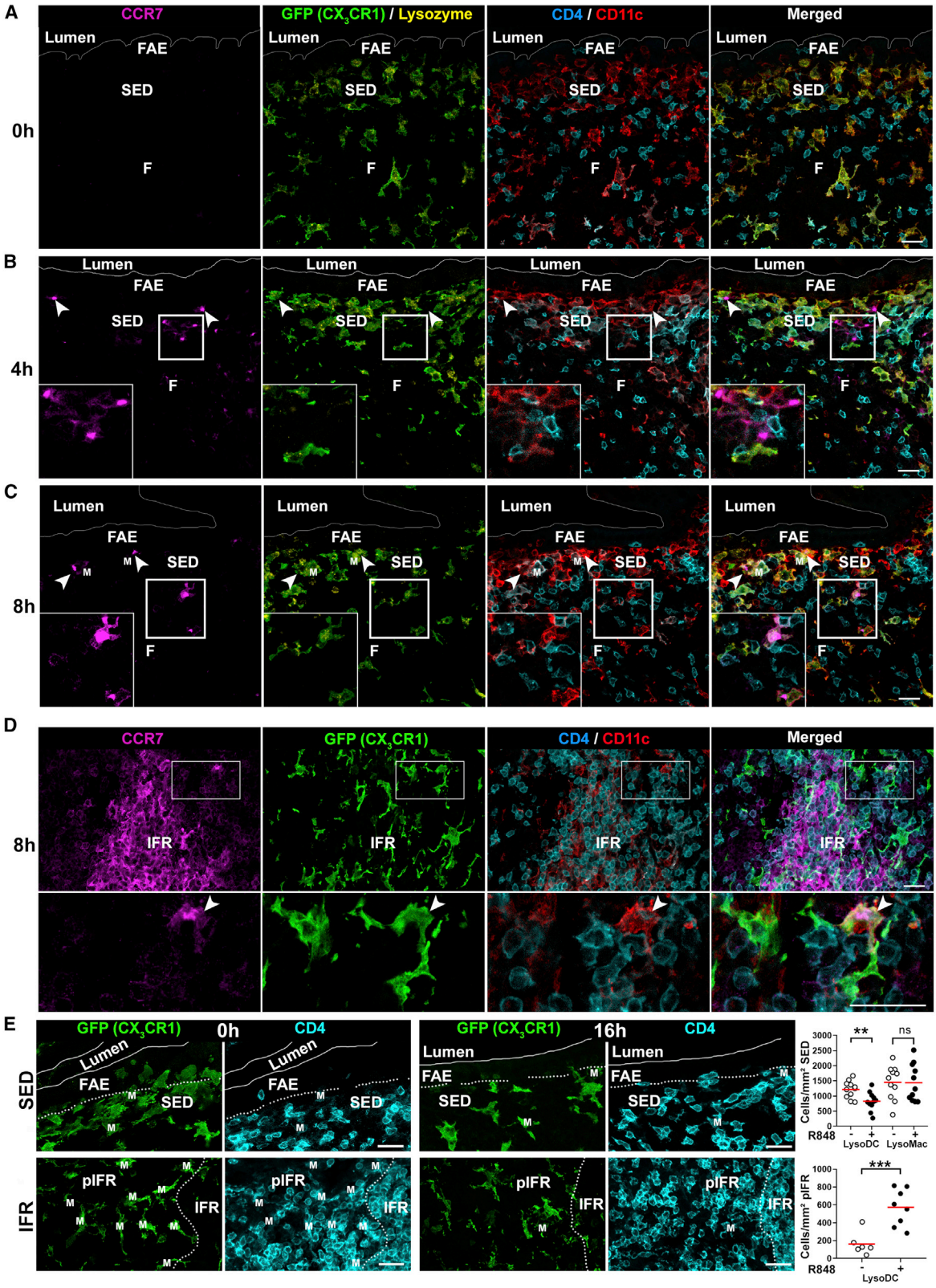

(legend on next page)

SUPPLEMENTAL INFORMATION

Supplemental Information can be found online at https://doi.org/10.1016/j.celrep.2020.03.043.

ACKNOWLEDGMENTS

We thank the histology, cytometry, and PICsL imaging core facilities for expert technical assistance; Violaine Alunni and Christelle Thibault from Plateforme Biopuces et sequençage de l'IGBMC (Strasbourg, France) for performing the microarray experiments; Pierre Milpied and Laurine Gil for helpful discussion and technical expertise in single-cell RNA sequencing; and Benjamin Harding for correcting the manuscript. This work was supported by institutional funding from Centre National de la Recherche Scientifique and Institut National de la Santé et de la Recherche Médicale, by the Agence Nationale de la Recherche grant ANR-10-INBS-04-01 France Bio Imaging, by the I2HD collaborative project developed jointly by CIML and Sanofi, and by the Fondation pour la Recherche Médicale (FRM) grant DEQ20170336745. C.D.S. and C.A.P. were supported by the FRM fellowship FDT20160434982 and the University of Costa Rica, respectively.

AUTHOR CONTRIBUTIONS

Conceptualization, H.L.; Methodology, C.W., J.B., C.D.S., and H.L.; Investigation, C.W., J.B., C.D.S., C.A.P., J.T., M.L., L.C., and H.L.; Formal Analysis, M.M., M.D., L.S., and H.L.; Resources, A.C.-N. and L.S.; Writing – Original Draft, H.L.; Writing – Review & Editing, C.W., J.B., C.D.S., M.D., L.S., H.L., and J.-P.G.; Supervision, Project Administration, and Funding Acquisition, H.L. and J.P.G.

DECLARATION OF INTERESTS

The authors declare no competing interests.

Received: October 15, 2019
Revised: February 7, 2020
Accepted: March 13, 2020
Published: April 7, 2020

REFERENCES

Amir, A.D., Davis, K.L., Tadmor, M.D., Simonds, E.F., Levine, J.H., Bendall, S.C., Shenfeld, D.K., Krishnaswamy, S., Nolan, G.P., and Pe'er, D. (2013). viSNE enables visualization of high dimensional single-cell data and reveals phenotypic heterogeneity of leukemia. Nat. Biotechnol. *31*, 545–552.

Ansel, K.M., Ngo, V.N., Hyman, P.L., Luther, S.A., Förster, R., Sedgwick, J.D., Browning, J.L., Lipp, M., and Cyster, J.G. (2000). A chemokine-driven positive feedback loop organizes lymphoid follicles. Nature *406*, 309–314.

Bonnardel, J., Da Silva, C., Henri, S., Tamoutounour, S., Chasson, L., Montañana-Sanchis, F., Gorvel, J.P., and Lelouard, H. (2015a). Innate and adaptive immune functions of peyer's patch monocyte-derived cells. Cell Rep. *11*, 770–784.

Bonnardel, J., Da Silva, C., Masse, M., Montañana-Sanchis, F., Gorvel, J.P., and Lelouard, H. (2015b). Gene expression profiling of the Peyer's patch mononuclear phagocyte system. Genom. Data *5*, 21–24.

Bonnardel, J., Da Silva, C., Wagner, C., Bonifay, R., Chasson, L., Masse, M., Pollet, E., Dalod, M., Gorvel, J.P., and Lelouard, H. (2017). Distribution, location, and transcriptional profile of Peyer's patch conventional DC subsets at steady state and under TLR7 ligand stimulation. Mucosal Immunol. *10*, 1412–1430.

Breitfeld, D., Ohl, L., Kremmer, E., Ellwart, J., Sallusto, F., Lipp, M., and Förster, R. (2000). Follicular B helper T cells express CXC chemokine receptor 5, localize to B cell follicles, and support immunoglobulin production. J. Exp. Med. *192*, 1545–1552.

Cera, M.R., Del Prete, A., Vecchi, A., Corada, M., Martin-Padura, I., Motoike, T., Tonetti, P., Bazzoni, G., Vermi, W., Gentili, F., et al. (2004). Increased DC trafficking to lymph nodes and contact hypersensitivity in junctional adhesion molecule-A-deficient mice. J. Clin. Invest. *114*, 729–738.

Da Silva, C., Wagner, C., Bonnardel, J., Gorvel, J.P., and Lelouard, H. (2017). The Peyer's patch mononuclear phagocyte system at steady state and during infection. Front. Immunol. *8*, 1254.

Depreter, M.G., Blair, N.F., Gaskell, T.L., Nowell, C.S., Davern, K., Pagliocca, A., Stenhouse, F.H., Farley, A.M., Fraser, A., Vrana, J., et al. (2008). Identification of Plet-1 as a specific marker of early thymic epithelial progenitor cells. Proc. Natl. Acad. Sci. U S A *105*, 961–966.

Dieu, M.C., Vanbervliet, B., Vicari, A., Bridon, J.M., Oldham, E., Aït-Yahia, S., Brière, F., Zlotnik, A., Lebecque, S., and Caux, C. (1998). Selective recruitment of immature and mature dendritic cells by distinct chemokines expressed in different anatomic sites. J. Exp. Med. *188*, 373–386.

Disson, O., Bleriot, C., Jacob, J.M., Serafini, N., Dulauroy, S., Jouvion, G., Fevre, C., Gessain, G., Thouvenot, P., Eberl, G., et al. (2018). Peyer's patch myeloid cells infection by Listeria signals through gp38^{+} stromal cells and locks intestinal villus invasion. J. Exp. Med. *215*, 2936–2954.

Förster, R., Mattis, A.E., Kremmer, E., Wolf, E., Brem, G., and Lipp, M. (1996). A putative chemokine receptor, BLR1, directs B cell migration to defined lymphoid organs and specific anatomic compartments of the spleen. Cell *87*, 1037–1047.

Figure 6. Subepithelial LysoDCs Upregulate CCR7 and Migrate at the Periphery of the IFR upon R848 Stimulation

(A–E) Spectral confocal imaging projections of PP from CX3CR1-GFP$^{-/+}$ mice taken before (A) and 4 h (B), 8 h (C and D), and 16 h (E) after R848 gavage and stained for GFP (green), CD11c (red), CD4 (cyan), and CCR7 (magenta).

(A) CCR7 was not expressed in the SED at steady state.

(B) CD11c^{+}CX$_3$CR1^{-} cells, arrowheads and boxed area) 4 h after R848 stimulation.

(C) CCR7 was expressed by subepithelial LysoDCs (CD11c^{+}CX$_3$CR1^{+}CD4^{-} cells, arrowheads and boxed area) but not LysoMacs (M, CD11c^{+}CX$_3$CR1^{+}CD4^{+} cells) 8 h after R848 stimulation.

(D) Recruitment of a CCR7-expressing LysoDC at the periphery of the IFR 8 h after R848 stimulation. Note that IFR-resident macrophages (CX$_3$CR1^{+}CD11c^{-}CD4^{-}, CX$_3$CR1^{+}CD11c^{-}CD4^{+}, and CX$_3$CR1^{+}CD11c^{+}CD4^{+} cells) did not express CCR7.

(E) Left: LysoDCs (CX$_3$CR1^{+}CD4^{-} cells) and LysoMacs (M; CX$_3$CR1^{+}CD4^{+} cells) in the SED (top panel) and at the IFR periphery (pIFR; bottom panel) following (right panel) or not (left panel) 16 h R848 treatment. Right: quantification of LysoDCs and LysoMacs in the SED (top) and of LysoDCs at the periphery of the IFR (pIFR; bottom) in PP taken from six or seven mice for each condition (ns, non-significant; $^{**}p < 0.01$ and $^{***}p < 0.001$, unpaired t test with Welch's correction). Bars, 20 μm. Pictures are representative of at least three independent experiments. See also Figures S5 and S6.

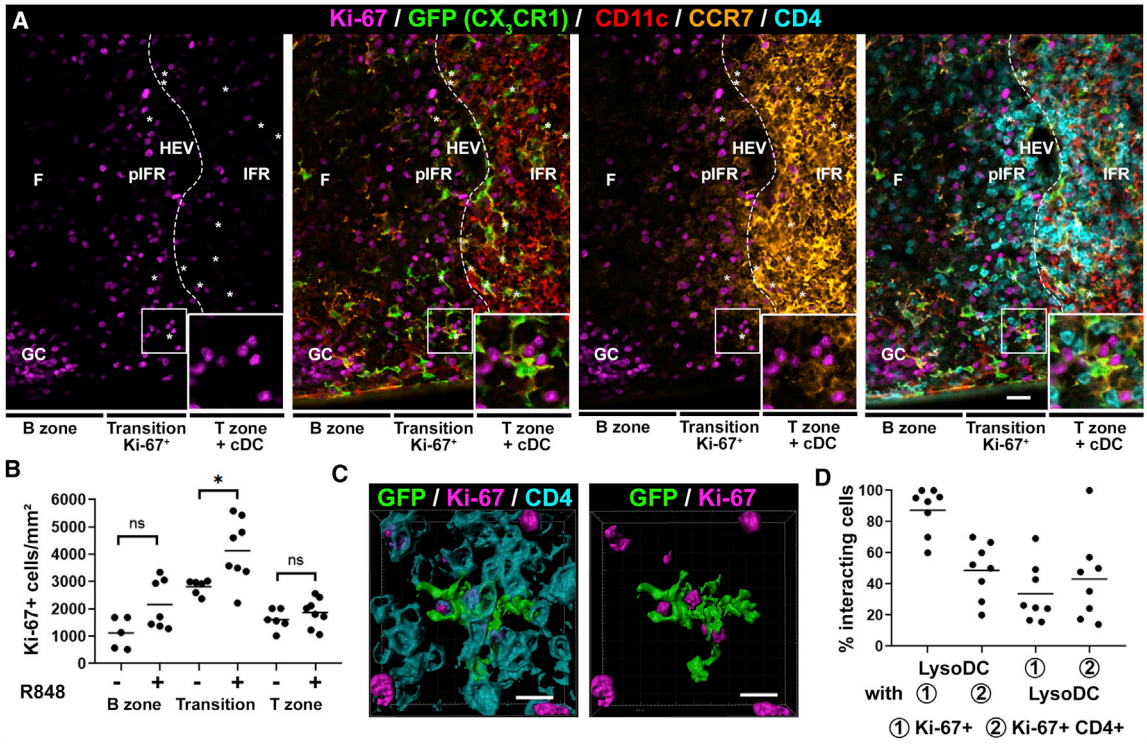

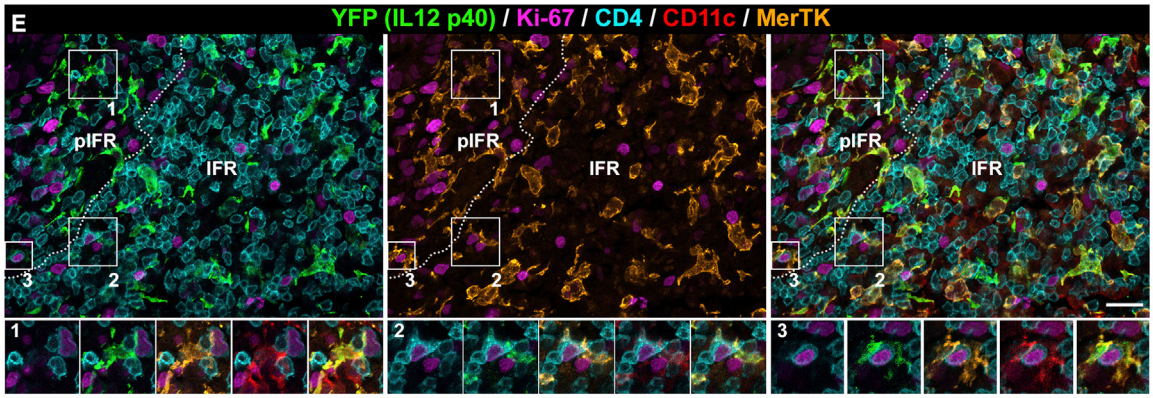

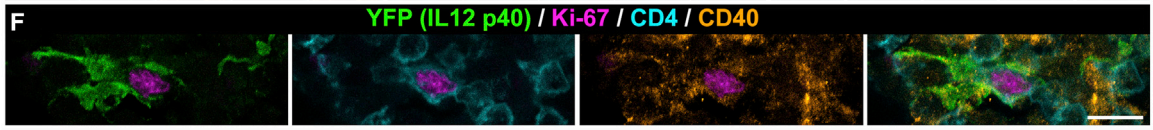

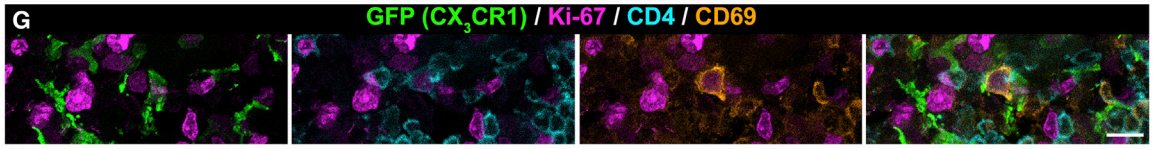

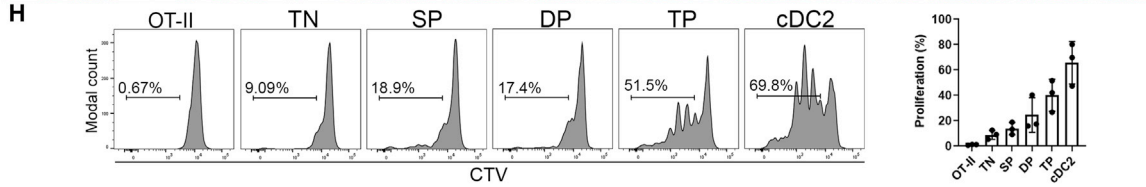

(legend on next page)

Förster, R., Schubel, A., Breitfeld, D., Kremmer, E., Renner-Müller, I., Wolf, E., and Lipp, M. (1999). CCR7 coordinates the primary immune response by establishing functional microenvironments in secondary lymphoid organs. Cell *99*, 23–33.

Gunn, M.D., Ngo, V.N., Ansel, K.M., Ekland, E.H., Cyster, J.G., and Williams, L.T. (1998). A B-cell-homing chemokine made in lymphoid follicles activates Burkitt's lymphoma receptor-1. Nature *391*, 799–803.

Iwasaki, A., and Kelsall, B.L. (2000). Localization of distinct Peyer's patch dendritic cell subsets and their recruitment by chemokines macrophage inflammatory protein (MIP)-3alpha, MIP-3beta, and secondary lymphoid organ chemokine. J. Exp. Med. *191*, 1381–1394.

Jung, S., Aliberti, J., Graemmel, P., Sunshine, M.J., Kreutzberg, G.W., Sher, A., and Littman, D.R. (2000). Analysis of fractalkine receptor CX(3)CR1 function by targeted deletion and green fluorescent protein reporter gene insertion. Mol. Cell. Biol. *20*, 4106–4114.

Jung, C., Hugot, J.P., and Barreau, F. (2010). Peyer's patches: the immune sensors of the intestine. Int. J. Inflamm. *2010*, 823710.

Karrich, J.J., Romera-Hernández, M., Papazian, N., Veenbergen, S., Cornelissen, F., Aparicio-Domingo, P., Stenhouse, F.H., Peddie, C.D., Hoogenboezem, R.M., den Hollander, C.W.J., et al. (2019). Expression of Plet1 controls interstitial migration of murine small intestinal dendritic cells. Eur. J. Immunol. *49*, 290–301.

La Manno, G., Soldatov, R., Zeisel, A., Braun, E., Hochgerner, H., Petukhov, V., Lidschreiber, K., Kastriti, M.E., Lönnerberg, P., Furlan, A., et al. (2018). RNA velocity of single cells. Nature *560*, 494–498.

Legler, D.F., Loetscher, M., Roos, R.S., Clark-Lewis, I., Baggiolini, M., and Moser, B. (1998). B cell-attracting chemokine 1, a human CXC chemokine expressed in lymphoid tissues, selectively attracts B lymphocytes via BLR1/CXCR5. J. Exp. Med. *187*, 655–660.

Lelouard, H., Henri, S., De Bovis, B., Mugnier, B., Chollat-Namy, A., Malissen, B., Meresse, S., and Gorvel, J.P. (2010). Pathogenic bacteria and dead cells are internalized by a unique subset of Peyer's patch dendritic cells that express lysozyme. Gastroenterology *138*, 173–184.e3.

Lelouard, H., Fallet, M., de Bovis, B., Meresse, S., and Gorvel, J.P. (2012). Peyer's patch dendritic cells sample antigens by extending dendrites through M cell-specific transcellular pores. Gastroenterology *142*, 592–601.e3.

Lelouard, H., Mailfert, S., and Fallet, M. (2018). A ten-color spectral imaging strategy to reveal localization of gut immune cell subsets.https://www.zeiss.fr/microscopie/service-assistance/notes-application/a-ten-color-spectral-imaging-strategy.html.

Liu, Z., Gu, Y., Chakarov, S., Bleriot, C., Kwok, I., Chen, X., Shin, A., Huang, W., Dress, R.J., Dutertre, C.A., et al. (2019). Fate mapping via Ms4a3-expression history traces monocyte-derived cells. Cell *178*, 1509–1525.e19.

Mabbott, N.A., Donaldson, D.S., Ohno, H., Williams, I.R., and Mahajan, A. (2013). Microfold (M) cells: important immunosurveillance posts in the intestinal epithelium. Mucosal Immunol. *6*, 666–677.

Macatonia, S.E., Hosken, N.A., Litton, M., Vieira, P., Hsieh, C.S., Culpepper, J.A., Wysocka, M., Trinchieri, G., Murphy, K.M., and O'Garra, A. (1995). Dendritic cells produce IL-12 and direct the development of Th1 cells from naive CD4+ T cells. J. Immunol. *154*, 5071–5079.

Martinez-Lopez, M., Iborra, S., Conde-Garrosa, R., Mastrangelo, A., Danne, C., Mann, E.R., Reid, D.M., Gaboriau-Routhiau, V., Chaparro, M., Lorenzo, M.P., et al. (2019). Microbiota sensing by Mincle-Syk axis in dendritic cells regulates interleukin-17 and -22 production and promotes intestinal barrier integrity. Immunity *50*, 446–461.e9.

Mellman, I., and Steinman, R.M. (2001). Dendritic cells: specialized and regulated antigen processing machines. Cell *106*, 255–258.

Murakami, M., Francavilla, C., Torselli, I., Corada, M., Maddaluno, L., Sica, A., Matteoli, G., Iliev, I.D., Mantovani, A., Rescigno, M., et al. (2010). Inactivation of junctional adhesion molecule-A enhances antitumoral immune response by promoting dendritic cell and T lymphocyte infiltration. Cancer Res. *70*, 1759–1765.

Ohno, H. (2016). Intestinal M cells. J. Biochem. *159*, 151–160.

Qiu, X., Mao, Q., Tang, Y., Wang, L., Chawla, R., Pliner, H.A., and Trapnell, C. (2017). Reversed graph embedding resolves complex single-cell trajectories. Nat. Methods *14*, 979–982.

Reinhardt, R.L., Hong, S., Kang, S.J., Wang, Z.E., and Locksley, R.M. (2006). Visualization of IL-12/23p40 in vivo reveals immunostimulatory dendritic cell migrants that promote Th1 differentiation. J. Immunol. *177*, 1618–1627.

Satpathy, A.T., Kc, W., Albring, J.C., Edelson, B.T., Kretzer, N.M., Bhattacharya, D., Murphy, T.L., and Murphy, K.M. (2012). Zbtb46 expression distinguishes classical dendritic cells and their committed progenitors from other immune lineages. J. Exp. Med. *209*, 1135–1152.

Figure 7. Mature LysoDCs Efficiently Prime Naive Helper T Cells *In Vitro* and Strongly Interact with Them at the Site of Their Proliferation upon Stimulation *In Vivo*

(A) Spectral confocal imaging projections of a PP from a CX3CR1-GFP$^{-/+}$ mouse 16 h after R848 gavage and stained for Ki-67 (magenta), GFP (green), CD11c (red), CCR7 (orange), and CD4 (cyan). Upon R848 stimulation, the IFR periphery (pIFR; transition area between the B and the T cell zones), delimited by a dashed line, was enriched in proliferating immune cells (Ki-67$^+$ cells in magenta), including helper T cells (CD4$^+$ cells in cyan). Many migratory LysoDCs (CD11c$^+$CX$_3$CR1$^+$CD4$^-$CCR7$^+$ cells, asterisks) were located in or next to the pIFR (i.e., more peripherally than IFR-located CD11c$^+$CX$_3$CR1$^-$CD4$^-$CCR7^{+++} cDCs). Higher magnification of the boxed area shows a migratory LysoDC strongly interacting with helper T cells and other immune cells, some of which were proliferating. Bar, 20 μm.

(B) Quantification of Ki-67$^+$ cells in the B (follicle), the T (IFR), and the transition area between the B and the T cell zone (pIFR) of PP taken from six or seven mice gavaged or not with R848 16 h earlier (ns, non-significant; *p < 0.05, unpaired t test with Welch's correction).

(C) Three-dimensional reconstruction of a R848-stimulated LysoDC (CX$_3$CR1$^+$CD4$^-$ cell, green) located at the IFR periphery and strongly interacting with several helper T cells (CD4$^+$, cyan; left panel), three of which were proliferating (Ki-67$^+$, pink; right panel). Bars, 10 μm.

(D) Ratio of LysoDCs interacting with (1) total proliferative cells (Ki-67$^+$) and (2) proliferative helper T cells (Ki-67$^+$CD4$^+$) and ratio of (1) total proliferative cells and (2) proliferative helper T cells interacting with LysoDCs at the periphery of the IFR.

(E and F) Spectral confocal imaging projections of the PP IFR/pIFR area from p40-IRES-eYFP mice 16 h after R848 gavage and stained for YFP (green), CD4 (cyan), Ki-67 (magenta), CD11c (red), and MerTK (E) or CD40 (F). (E) Higher magnifications of the numbered boxed areas show three IL-12 p40-expressing LysoDCs (YFP$^+$CD11c$^+$MerTK$^+$CD4$^-$) strongly interacting with helper T cells, some of which were proliferating. Bar, 20 μm.

(F) CD40 was enriched at the contact zone between two IL-12 p40-expressing LysoDCs and a proliferating helper T cell. Bar, 10 μm.

(G) A proliferating helper T cell in tight interaction with a LysoDC (CX$_3$CR1$^+$CD4$^-$ cell) strongly expressed CD69. Bar, 10 μm.

(H) PP phagocytes were sorted as shown in Figure S1C. Each sorted LysoDC subset and CD11b$^+$ cDC2 were incubated with ovalbumin before co-culture with OT-II T cells for 4 days. The latter were gated as SSC^{low}FSC^{low} and Vα2$^+$CD4$^+$ live cells, and their proliferation was measured as a loss of CTV staining. Only TP LysoDCs and cDC2 were able to efficiently prime naive T cells. Histograms are representative of the three independent experiments summarized on the right.

In (A)–(G), pictures are representative of at least three independent experiments.

See also Figures S6 and S7 and Video S2.

Schaerli, P., Willimann, K., Lang, A.B., Lipp, M., Loetscher, P., and Moser, B. (2000). CXC chemokine receptor 5 expression defines follicular homing T cells with B cell helper function. J. Exp. Med. *192*, 1553–1562.

Tang, H.L., and Cyster, J.G. (1999). Chemokine up-regulation and activated T cell attraction by maturing dendritic cells. Science *284*, 819–822.

van der Maaten, L., and Hinton, G. (2008). Visualizing data using t-SNE. J. Mach. Learn. Res. *9*, 2579–2605.

Wagner, C., Bonnardel, J., Da Silva, C., Martens, L., Gorvel, J.P., and Lelouard, H. (2018). Some news from the unknown soldier, the Peyer's patch macrophage. Cell. Immunol. *330*, 159–167.

Yrlid, U., Milling, S.W., Miller, J.L., Cartland, S., Jenkins, C.D., and MacPherson, G.G. (2006). Regulation of intestinal dendritic cell migration and activation by plasmacytoid dendritic cells, TNF-alpha and type 1 IFNs after feeding a TLR7/8 ligand. J. Immunol. *176*, 5205–5212.

STAR★METHODS

KEY RESOURCES TABLE

REAGENT or RESOURCE	SOURCE	IDENTIFIER
Antibodies		
Rat anti-PLET1 unlabeled	Provided by C. Blackbrun	(Depreter et al., 2008)
Rabbit anti-lysozyme unlabeled	Dako	RRID:AB_303050
Chicken anti-GFP	Aveslab	RRID:AB_2307313
Rat anti-JAM-A unlabeled	Santa Cruz Biotechnology	RRID:AB_629830
Rat anti-CD101 unlabeled	ThermoFisher	RRID: AB_2610570
Goat anti-CD69 unlabeled	Bio-Techne	RRID:AB_416586
Rat anti-CD40 unlabeled	Bio-Rad	RRID:AB_323810
Rat anti-embigin unlabeled	eBioscience	RRID:AB_2016582
Rat anti-MerTK unlabeled	eBioscience	RRID:AB_2688282
Hamster anti-CD11c unlabeled	Biolegend	RRID:AB_313771
Rat anti-CCR7 unlabeled	Biolegend	RRID:AB_389229
Rat anti-CD205 unlabeled	Biolegend	RRID:AB_2281398
Rat anti-CD4 eFluor 405	eBioscience	RRID:AB_1272194
Rat anti-CD45.1 eFluor 405	eBioscience	RRID:AB_1272189
Rat anti-Ki-67 eFluor 660	eBioscience	RRID:AB_2574235
Anti-MHCII AF488	BD Biosciences	Cat# 562352
Anti-CD24 AF647	Biolegend	RRID:AB_493484
Anti-EpCam AF647	Biolegend	RRID:AB_1134101
Anti-CD45.2 AF647	Biolegend	RRID:AB_492870
Anti-BST2 APC	Biolegend	RRID:AB_1967127
Anti-CD11c Pe-Cy7	Biolegend	RRID:AB_493568
Anti-CD4 Pe-Cy5.5 or BUV737	eBioscience or BD Biosciences	RRID:AB_11218300 or Cat# 612843
Anti-embigin PE	eBioscience	RRID:AB_2016706
Anti-MHCII AF700	eBioscience	RRID:AB_494009
Anti-Jam-A biotin	Bio-Rad	RRID:AB_567268
Anti-CD24 BV421	BD Biosciences	Cat# 562789
Anti-CD172a FITC	BD Biosciences	RRID:AB_1645240
Anti-Va2 FITC	BD Biosciences	RRID:AB_394759
Streptavidin PE-CF594	BD Biosciences	RRID:AB_11154598
Rabbit anti-CD172a unlabeled	Bio-Rad	RRID:AB_322747
Goat anti-TIM-4 unlabeled	Bio-Techne	RRID:AB_2240431
Mouse anti-CD11c unlabeled or FITC	BD Bioscience	RRID:AB_393646 or Cat# 561355
Mouse anti-CD163 unlabeled	BD Bioscience	RRID:AB_396295
Mouse anti-CD24 unlabeled	BD Bioscience	RRID:AB_395820
Mouse anti-HLA-DR unlabeled	BD Bioscience	RRID:AB_396144
Mouse anti-CD20 unlabeled	BD Bioscience	RRID:AB_395987
Mouse anti-CD1c unlabeled	Biolegend	RRID:AB_1088995
Mouse anti-JAM-A unlabeled	eBioscience	RRID:AB_795873
Mouse anti-CD4 unlabeled	eBioscience	RRID:AB_2572867
Goat anti-mouse IgG1 AF488	Jackson Immunoresarch	RRID:AB_2338854
Goat anti-mouse IgG1 Cy3	Jackson Immunoresarch	RRID:AB_2338694
Goat anti-mouse IgG2b Cy3	Jackson Immunoresarch	RRID:AB_2338696
Goat anti-mouse IgG2a AF594	Jackson Immunoresarch	RRID:AB_2338886

(*Continued on next page*)

Continued

REAGENT or RESOURCE	SOURCE	IDENTIFIER
Goat anti-Armenian hamster IgG AF594	Jackson Immunoresarch	RRID:AB_2338999
Goat anti-Armenian hamster IgG Cy3	Jackson Immunoresarch	RRID:AB_2338989
Donkey anti-chicken IgG AF488	Jackson Immunoresarch	RRID:AB_2340375
Donkey anti-rat IgG Cy3	Jackson Immunoresarch	RRID:AB_2340667
Donkey anti-chicken IgG AF488	Jackson Immunoresarch	RRID:AB_2340375
Goat anti-rabbit IgG AF514	ThermoFisher	RRID:AB_2536173
Biological Samples		
Human Peyer's patch from patients undergoing surgery for colon cancer	Pathological anatomy and cytology laboratory, Marseille FRANCE	N/A
Chemicals, Peptides, and Recombinant Proteins		
R848 (resiquimod)	InvivoGen	Cat# tlrl-r848-5
Collagenase II	Worthington	Cat# CLS-2
DNase I	Sigma-Aldrich	Cat# DN25-1G
Antigenfix	Microm Microtech	Cat# F/P0014
Fixable Viability Dye eFluor 506	ThermoFisher	Cat# 65-0866-14
Fc Block (2.4G2, culture supernatant)	In house	N/A
Alcian Blue 8GX	Sigma-Aldrich	A3157
RPMI-1640	GIBCO	Cat# 21875034
Fetal Bovine Serum (South America)	Pan Biotech	Cat# P30-3306
GM-CSF (culture supernatant)	In house	N/A
M-CSF (culture supernatant)	In house	N/A
Penicillin/Streptomycin	GIBCO	Cat# 15140122
HEPES	GIBCO	Cat# 15630080
Sodium pyruvate	GIBCO	Cat# 11360039
L-Glutamine	GIBCO	Cat# 25030024
MEM non-essential amino acids solution	Sigma	Cat# M7145-100ML
2-Mercaptoethanol	GIBCO	Cat# 31350010
Fluoresbrite® BB carboxylate microspheres 0.5μm	PolySciences, Inc	Cat# 18339-10
CellTrace Violet	Life Technologies	Cat# C34557
EndoFit Ovalbumin	InvivoGen	Cat# vac-pova
Critical Commercial Assays		
Alexa Fluor 647 Protein Labeling Kit	ThermoFisher	Cat# A20173
Anti-mouse CD11c microbeads	Miltenyi Biotec	Cat# 130-108-338
CD4+ T cell negative isolation kit	Miltenyi Biotec	Cat# 130-104-454
RNeasy PLUS micro kit	QIAGEN	Cat# 74034
GeneChip® Mouse Gene 1.0 ST array	Affymetrix	Cat# 901168
Chromium Single Cell 3′ v2 kit	10X Genomics	Cat# PN-120267
LIVE/DEAD Fixable Blue Dead Cell Stain Kit	ThermoFisher	Cat# L23105
Deposited Data		
Microarray data of C57BL/6 Peyer's patch phagocytes	Bonnardel et al., 2015a, 2017 and this paper	GEO: GSE65514, GEO: GSE94380, GEO: GSE133864
Sc-RNA-Seq raw data of C57BL/6 LysoDC	This paper	GEO: GSE141776
Experimental Models: Organisms/Strains		
Mouse: C57BL/6	In-house colony	N/A
Mouse: C57BL/6	Janvier Labs	https://www.janvier-labs.com/en/
Mouse: CXCR5−/−	Jackson Laboratory	Jax stock 006659
Mouse: p40-IRES-eYFP	Jackson Laboratory	Jax stock 006412

(*Continued on next page*)

Continued

REAGENT or RESOURCE	SOURCE	IDENTIFIER
Mouse: CX3CR1-GFP	Jackson Laboratory	Jax stock 005582
Mouse: OT-II kept on rag1−/− X B6 (CD45.1)	Jackson laboratory	Jax stock 004194
Mouse: Zbtb46-GFP	Jackson Laboratory	Jax stock 027618
Software and Algorithms		
FlowJo v10	FlowJo, Treestar Inc.	https://www.flowjo.com/solutions/flowjo RRID:SCR_008520
BD FACSDiva v8	BD Biosciences	https://www.bdbiosciences.com/en-us/
Adobe Photoshop CS6	Adobe Systems Inc.	https://www.adobe.com RRID:SCR_014199
ZEN Lite 2.3 SP1	Carl Zeiss Microscopy	https://www.zeiss.com/microscopy/us/products/microscope-software/zen-lite.html RRID:SCR_013672
Imaris, v8	Oxford Instruments Group	https://imaris.oxinst.com/ RRID:SCR_007370
Prism, v8	GraphPad Software	https://www.graphpad.com/scientific-software/prism/ RRID:SCR_002798
Other		
LSR-II UV flow cytometer	BD Biosciences	N/A
ARIA-III cell sorter	BD Biosciences	N/A
AutoMACS Pro	Miltenyi Biotec	N/A
LS Columns	Miltenyi Biotec	Cat# 130-042-401
LSM 780 confocal microscope	Carl Zeiss Microscopy	N/A
BioAnalyzer	Agilent	Cat# G2939BA

LEAD CONTACT AND MATERIALS AVAILABILITY

Further information and requests may be directed to and will be fulfilled by the lead contact: Hugues Lelouard (lelouard@ciml.univ-mrs.fr). This study did not generate new unique reagents.

EXPERIMENTAL MODEL AND SUBJECT DETAILS

6–10 week-old C57BL/6Rj female mice were from Janvier Labs. CXCR5$^{-/-}$, p40-IRES-eYFP (Yet40), Zbtb46^{gfp} and CX3CR1-GFP female mice have been previously described (Förster et al., 1996; Jung et al., 2000; Reinhardt et al., 2006; Satpathy et al., 2012). Mice were maintained at our animal house facility in ventilated cages under specific pathogen free conditions at an ambient temperature of 22°C with a 12h light/dark cycle. The French ethical committee approved all animal studies. Redundant, surgically resected human PP specimens were obtained from patients undergoing surgery for colon cancer with their informed consent.

METHOD DETAILS

R848 treatment

Mouse gavage was performed with 10 μg of R848 (Invivogen) in 100 μL of sterile PBS.

Antibodies

Anti-mouse Antibodies: Rat monoclonal anti-PLET1 antibody (clone 1D4) was a kind gift from C. Blackburn (Depreter et al., 2008). Polyclonal rabbit anti-lysozyme (mouse and human) was from Dako and coupled to Alexa Fluor 647 according to manufacturer's instructions (Invitrogen). Chicken anti-GFP was from Aveslab. Monoclonal rat antibody anti-JAM-A (clone BV12) was from Santa Cruz Biotechnology. Monoclonal rat antibody anti-CD101 (clone 307707) and polyclonal goat antibody anti-CD69 were from Bio-Techne. Monoclonal rat antibody anti-CD40 (clone 3/23) was from Bio-Rad. Monoclonal rat antibodies anti-embigin (clone G7.43.1) and anti-MerTK (clone DS5MMER) were from eBioscience. Monoclonal hamster antibody anti-CD11c (clone N418) and rat antibodies anti-CCR7 (clone 4B12) and anti-CD205 (NLDC-145) were from Biolegend. Monoclonal rat antibodies anti-CD4 (clone RM4-5) and anti-CD45.1 (clone A20) coupled to eFluor 450 and Ki-67 (clone SolA15) coupled to eFluor 660 were from eBioscience. Monoclonal

antibody anti-MHCII (clone M5/114) coupled to Alexa Fluor 488 was from BD Biosciences. Monoclonal antibodies anti-CD24 (clone M1/69), anti-EpCAM (clone G8.8) and anti-CD45.2 (clone 104) coupled to Alexa Fluor 647 were from Biolegend. For cytometry, BST2 (APC; clone 927), CD11c (PE-Cy7; N418) were purchased from Biolegend. CD4 (PE-Cy5.5; clone RM4-5), embigin (PE; clone G7.43.1) and MHCII (Alexa Fluor 700; clone M5/114.15.2) were from eBioscience; JAM-A (biotin; clone H202-106) was from Bio-Rad; CD24 (BV421; clone M1/69), SIRPα (FITC; clone P84), Vα2 TCR (FITC; clone B20.1), CD4 (BUV737; clone RM4-5) and Streptavidin-PE-CF594 for detection of biotin from BD Biosciences.

Anti-human Antibodies: Polyclonal rabbit anti-SIRPα antibody was from Bio-Rad. Polyclonal goat anti-TIM-4 antibody was from Bio-Techne. Mouse IgG_1 anti-CD11c (clone B-ly6; uncoupled or coupled to FITC), IgG_1 anti-CD163 (clone GHI/61), IgG_{2a} anti-CD24 (clone ML5), IgG_{2a} anti-HLA-DR (clone G46-6) and IgG_{2b} anti-CD20 (clone 2H7) were from BD Biosciences. Mouse IgG_1 anti-CD1c (clone L161) was from Biolegend. Mouse IgG_1 anti-JAM-A (clone WK9) and IgG_{2b} anti-CD4 (clone N1UG0) were from eBioscience.

Control and secondary antibodies: Alexa Fluor secondary antibodies were from ThermoFisher Scientific except goat anti-mouse IgG_1, IgG_{2a} and IgG_{2b}, Cy3 and Alexa Fluor 594 Goat anti-hamster and control antibodies from Jackson Immunoresearch.

Immunofluorescence staining and confocal microscopy

PP were fixed with Antigenfix (Diapath) for 1 h, washed and processed as previously described (Lelouard et al., 2012). Slides were observed with a Zeiss LSM 780 confocal microscope using the spectral imaging mode (Lelouard et al., 2018). Images were analyzed using Adobe Photoshop CS6 and Imaris.

PP cell extraction

PP were digested for 40 min at room temperature with collagenase/DNase as previously described (Bonnardel et al., 2015b). All subsequent procedures were at 0–4°C. $CD11c^+$ cells were sorted using anti-CD11c microbeads and an AutoMACS magnetic cell separator according to manufacturer's instructions (Miltenyi Biotec).

Flow cytometry and cell sorting

$CD11c^+$ cells were preincubated on ice for 10 min with 2.4G2 antibody to block Fc receptors and stained for surface markers. Cell viability was evaluated using Fixable Viability Dye eFluor 506 or LIVE/DEAD Fixable Blue Dead Cell Stain Kit (Life Technologies). Multiparameter flow cytometry and cell sorting were performed using a FACS LSRII and a FACSAria III (BD Biosciences), respectively. Data were analyzed with Flow Jo and BD FACSDiva softwares.

In vitro LysoDC subset culture

Sorted LysoDC were coated on 1% Alcian blue treated coverslips or put in 96-well plate (1.500 cells/well) and incubated at 37°C, 5% CO_2 for 1 hour in culture medium (RPMI-1640 supplemented with 10% fetal calf serum (FCS), 1% GM-CSF, 10% M-CSF, 1% penicillin/streptomycin, 10 mM HEPES, 1 mM sodium pyruvate, 1 mM glutamine, 1 mM non-essential amino-acids, and 50 μM 2-ME) containing or not 10 μg R848. For *in vitro* phagocytosis, they were incubated in presence of 0.5 μM Fluoresbrite Bright Blue microspheres (Polysciences) for an additional hour. Cells were fixed and stained for microscopy. Cells cultured in 96-well plate were incubated with Fixable Viability Dye eFluor 506 (Life Technologies) for 10 min and phagocytosis was evaluated using a FACS LSRII. For priming of helper T cells, OT-II T cells were isolated from lymph nodes of OT-II $rag1^{-/-}$ mice using a $CD4^+$ T cell-negative isolation kit (Miltenyi) and incubated with 1 μM CellTrace Violet (CTV; Life Technologies) for 12 min at 37°C. 2.5×10^4 CTV-labeled OT-II T cells were cultured together with sorted 2.5×10^3 LysoDC or cDC2 pulsed for 2 hr at 37°C with 200 μg/ml endotoxin-free OVA (EndoFit Ovalbumin; Invivogen). On the 4^{th} day of co-culture, T cells proliferation was measured as a loss of CTV staining.

Microarray analysis

The total RNA of PP-sorted phagocytes from 3 to 5 independent experiments was extracted with a QIAGEN RNAeasy PLUS micro kit. Quantity, quality and absence of genomic DNA contamination were assessed with a Bioanalyzer (Agilent). Microarray experiments were performed by the Plateforme Biopuces of Strasbourg (Strasbourg, France) using the GeneChip® Mouse Gene 1.0 ST array (Affymetrix). Quality controls and normalization of array data were performed as previously described (Bonnardel et al., 2015b). Data were normalized with our previous gene array data deposited under the accession number GEO: GSE65514 by Robust Multi-chip Analysis.

Single cell RNA-sequencing analysis

Next generation sequencing was performed by HalioDX (Marseille, France) using the Chromium Single Cell 3′ kit from 10X genomics (California, USA) for the library preparation and the NextSeq 500/550 High Output Kit v2 (75 cycles) cartridges from Illumina for the sequencing. FASTQ raw files were processed using Cell Ranger software (v2.1.1, default parameters), which performs alignment, filtering, barcode counting and unique molecular identifier (UMI) counting. Reads were aligned to the mouse mm10 genome.

Quality control and cell filtering: a total number of 8,499 cells were identified with a mean of 56,659 reads per cell and a median of 2,364 genes per cell. Quality control (QC) was performed to remove poor quality cells thanks to in-house developed R scripts. Using Seurat R package CreateSeuratObject function, cells with less than 200 or more than 5000 (potential doublets) detected genes, cells

with low number of UMI (log10 (UMI) < 3.3) and cells with more than 40% mitochondrial gene expression (apoptotic cells) were removed. The first QC removed only 30 cells and 8,469 cells remained available for analysis indicating the good quality of the sample. Expression data were normalized using the Seurat R package NormalizeData function (using logNormalize method and scale factor of 10000). Using PCA (see below), we observed a dependency in number of UMI in the first principal component. We centered and regressed the expression data from that factor using the Seurat R package ScaleData function (centering true and scaling false). Using Seurat clustering method, we observed a specific cluster of 86 cells with a gene signature identifying them as contamination. Then, using the Pagoda2 clustering method (see below) we observed a cluster of 381 cells enriched in expression of mitochondrial genes identified as dying cells and two clusters of 65 and 173 cells with gene signatures identifying them as contamination. At the end of the quality control procedures, a total number of 643 cells were removed from the analysis.

Dimensionality reduction and clustering: principal component analysis (PCA) was run using dudi.pca function from ade4 R package with data centering. The t-distributed stochastic neighbor embedding (t-SNE) implemented via Barnes-Hut approximations (bh-SNE), was run using Rtsne function of Rtsne R package (perplexity = 30, and default option values). Clustering was done using two methods: (i) Seurat FindClusters based on PCA dimensionality reduction and the 10 first principal components; (ii) getKnnClusters function from Pagoda2 R package taking advantage of the Multilevel and Walktrap community detection method.

Pseudo-time analysis: We used standard protocol as described in the tutorial of the Monocle2 R package (v 2.6.4; see http://cole-trapnell-lab.github.io/monocle-release/docs/) and in-house developed R scripts. Briefly, we started by defining custom cell types as described below ("-" indicates the gene expression count must be 0, "+" indicates the gene expression count must be at least 1):

SP = $Ccne1^{-}$ $Mcm6^{-}$ $Cenpa^{-}$ $Ccnb2^{-}$ Emb^{+} $Trem3^{+}$ $F11r^{-}$ $Cd24a^{-}$ $Plet1^{-}$ $Tspan10^{-}$ $Apoc4^{-}$
DP = Emb^{+} $F11r^{+}$ $Plet1^{-}$ $Tspan10^{-}$
TP = Emb^{+} $F11r^{+}$ $Plet1^{+}$ $Tspan10^{-}$
TN = $Ccne1^{-}$ $Mcm6^{-}$ $Cenpa^{-}$ $Ccnb2^{-}$ Emb^{-} $Trem3^{-}$ $F11r^{-}$ $Cd24a^{-}$ $Plet1^{-}$ $Clec4d^{-}$ $Tspan10^{+}$ $Apoc4^{+}$

These cell types were used to classify cells according to the classifyCells function of the Monocle2 package. On a total number of 7,659 cells (high quality minus proliferative cells), 1693 cells were classified (630 SP, 640 DP, 157 TP, 266 TN). Using the calculateMarkerSpecificity function of Monocle2, we computed the best markers among the different cell types and selected the top 50 genes, which were used to order the cells along the pseudo-time thanks to the orderCells function of Monocle2.

Using the plotCellTrajectory function of Monocle2, we obtained the minimum spanning tree of cells ordered with pseudo-time. The origin of pseudo-time was chosen according to the previous analysis. Pseudo-time computation was done in order to keep the length of pseudo-time values along the various branches.

RNA velocity analysis: Analysis was done using the velocyto tool in two steps: first, python implementation with the velocyto run CLI to produce a loom file with the model computation; second, use of the velocyto and Pagoda2 R packages both with in-house developed scripts to produce further analysis from the obtained loom file, following Kharchenko Lab documentation. Cell velocity flow was mapped on the t-SNE map using the show.velocity.on.embedding.cor function of the velocyto R package (arrow.lwd = 1, n = 300, arrow.scale = 20, grid.n = 30). single cell velocities flow mapped on the t-SNE map produced at the previous steps showed very good agreement (both qualitatively and quantitatively) with the pseudo-time analysis plotted on the same t-SNE embedding.

QUANTIFICATION AND STATISTICAL ANALYSIS

Results were compared with GraphPad Prism 6 software using unpaired t test with Welch's correction. All experimental points are shown in the figures. Number of experiments, group sizes and statistical significance are given in the figure legends.

DATA AND CODE AVAILABILITY

The accessions numbers for the microarray and scRNA-seq data reported in this paper are GEO: GSE133864 and GEO: GSE141776, respectively. In house-made code, original data and corresponding docker images are available from the project github repository (https://github.com/CIML-bioinformatic/LysoDC) both with a readme explaining the detailed procedure to reproduce the results.